Karlsruhe Institute of Technology

Advanced Functional Inorganic POMs, Coordination Clusters and Framework Materials

Dr. Masooma Ibrahim

Institute of Nanotechnology (INT)

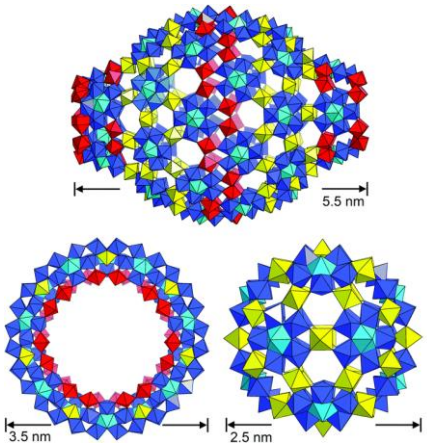

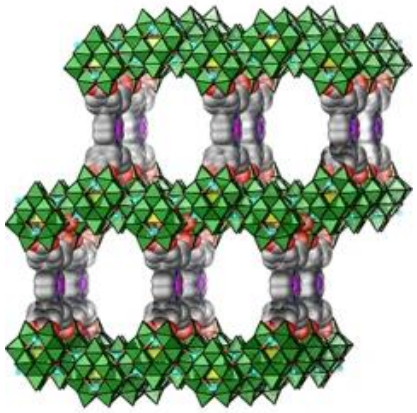

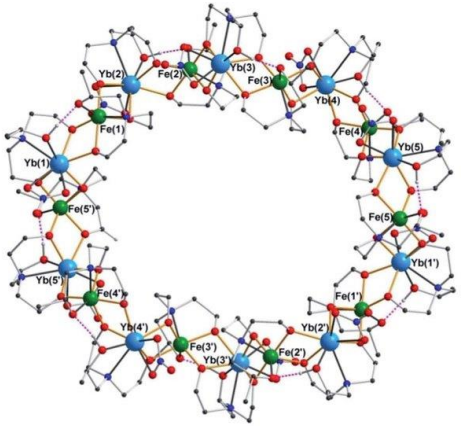

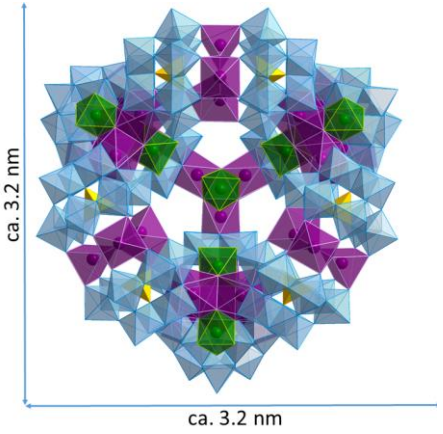

Solid State Characterization Techniques

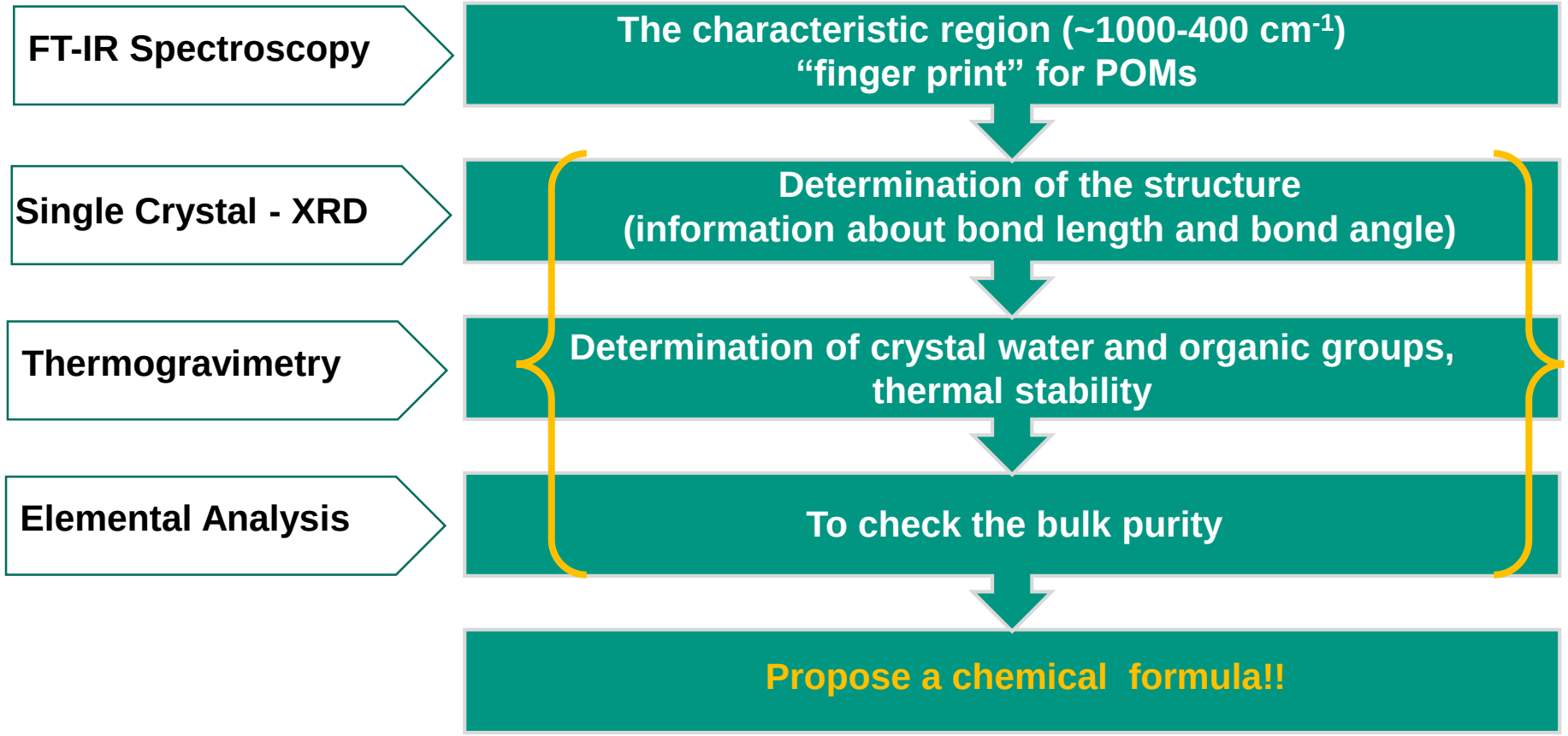

Solid State Characterization Techniques

Example:

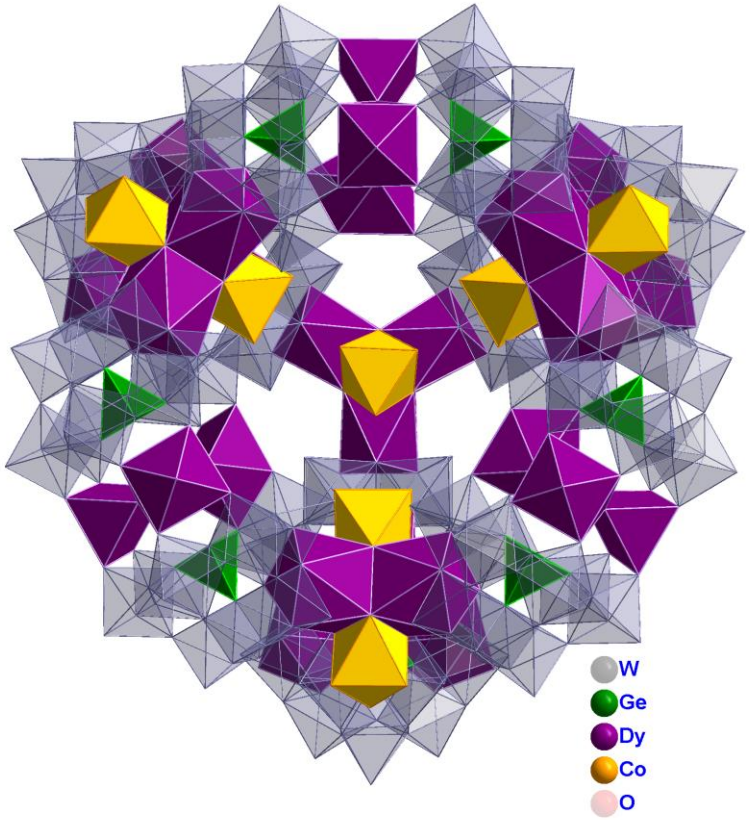

$Cs_{14}Na_{30}Co^{II}_{6}[\{(GeW_9O_{34})_2Dy^{III}_{3}(\mu_2\text{-}OH)_3(H_2O)_2\}_6\{Co^{II}_{2}Dy^{III}_{3}(\mu_3\text{-}OH)_6(OH_2)_6\}_4]\cdot 370H_2O$

$\{Dy_{30}Co_8\}$

M. Ibrahim, V. Mereacre, N. Leblanc, W. Wernsdorfer, C. E. Anson, A. K. Powell, *Angew. Chem. Int. Ed,* ***2015***, 54, 15574.

Solution State Characterization Techniques

Stability and structural information

- Multinuclear NMR Spectroscopy
- UV-Vis Spectroscopy
- Cyclic Voltammetry
- Mass Spectrometry

Solid State Characterization Techniques

FT-IR Spectroscopy

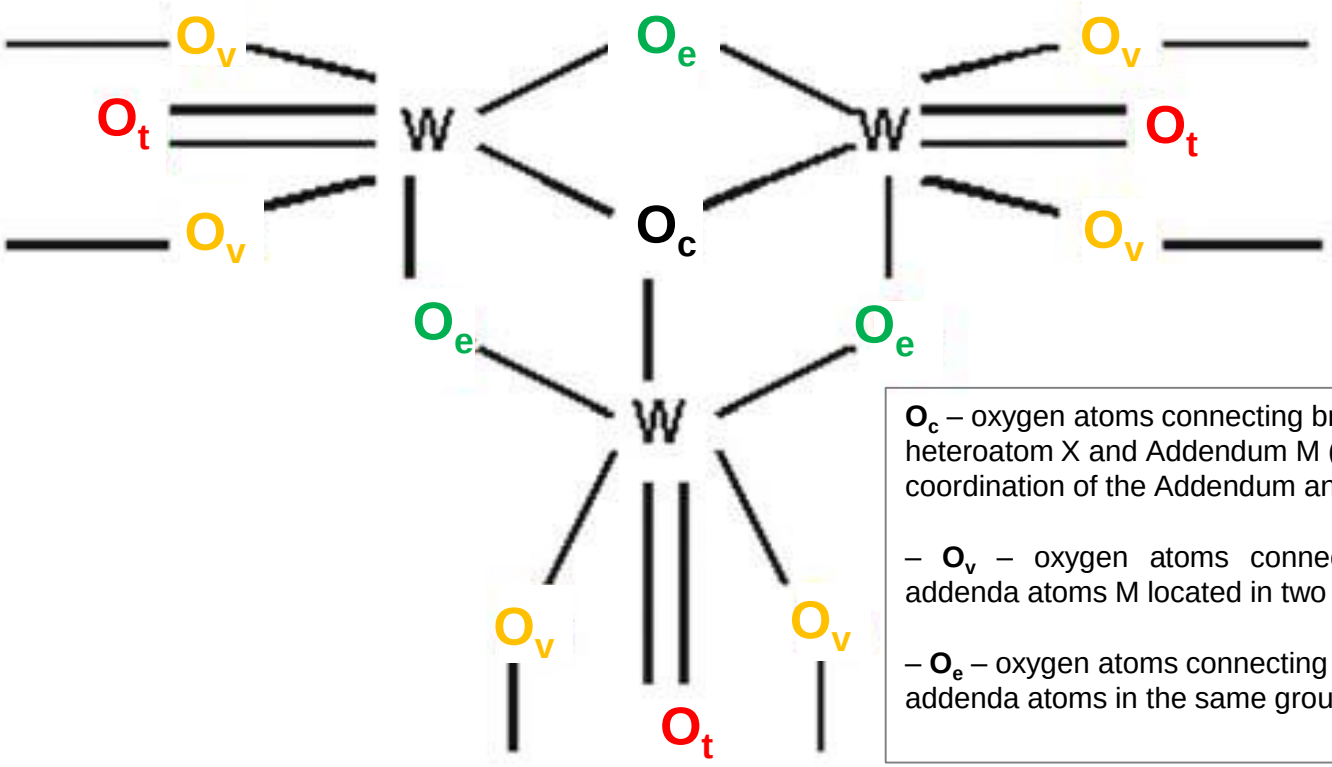

O_c – oxygen atoms connecting bridge between the heteroatom X and Addendum M (common both octahedron coordination of the Addendum and heteroatom X polyhedron)

– **O_v** – oxygen atoms connecting bridge between two metal addenda atoms M located in two different sets of triplets M_3O_{13}

– **O_e** – oxygen atoms connecting bridge between two addenda atoms in the same group M_3O_{13};

Types of addendum-oxygen connections in polyoxometalates

Solid State Characterization Techniques

FT-IR Spectroscopy: $Na_3[PW_{12}O_{40}]\cdot H_2O$

Edge-sharing oxygen atoms **(W−O_e−W)**
Vertex/corner-sharing oxygen atoms **(W−O_v−W)**
Terminal oxygen atoms **(W − O_t)**
P-Oc

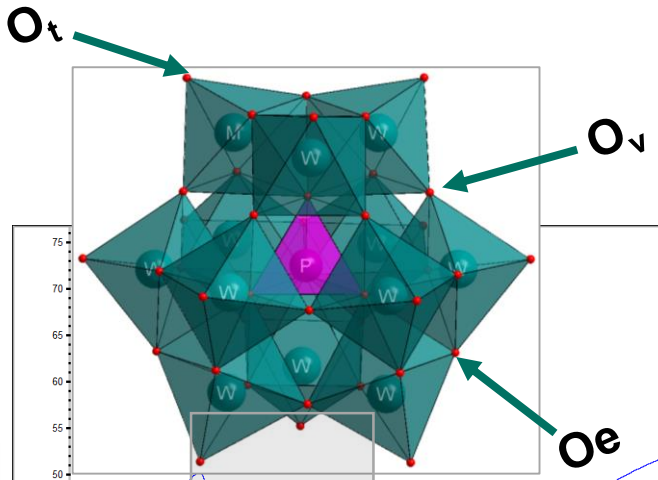

FT-IR Spectroscopy

$[Cu(cyclam)]_2[\{Cu(cyclam)\}_4\{(\alpha\text{-}GeW_{11}O_{39})Ln(H_2O)(OAc)\}_2]\cdot 18H_2O$ (**1-Ln**, where Ln = La–Lu

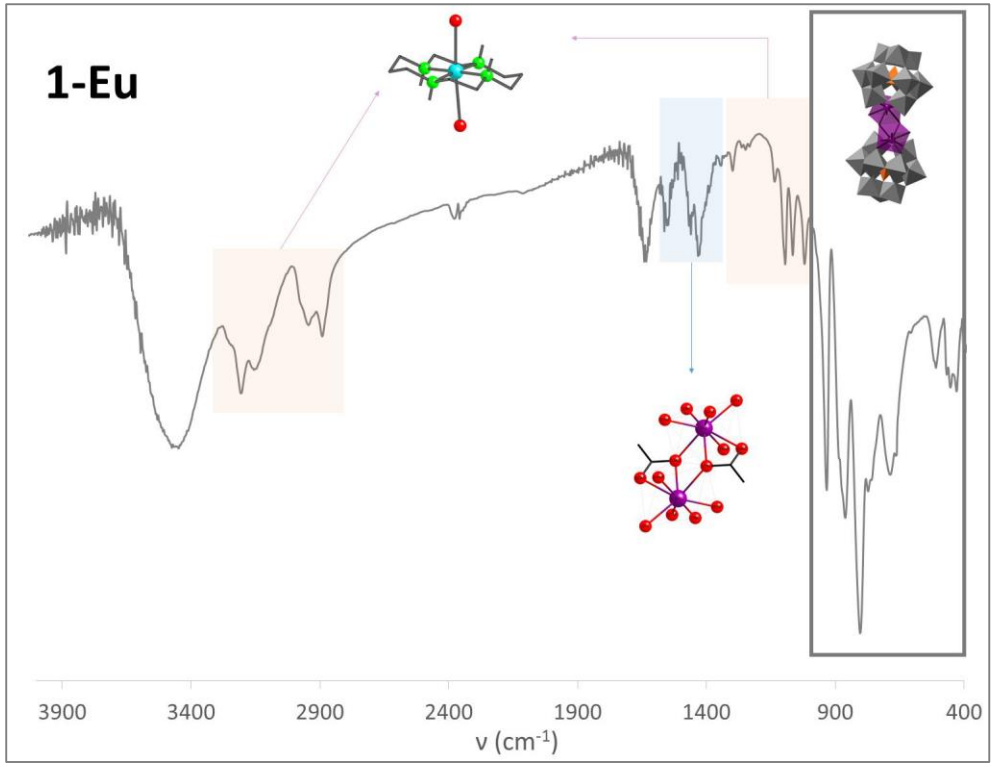

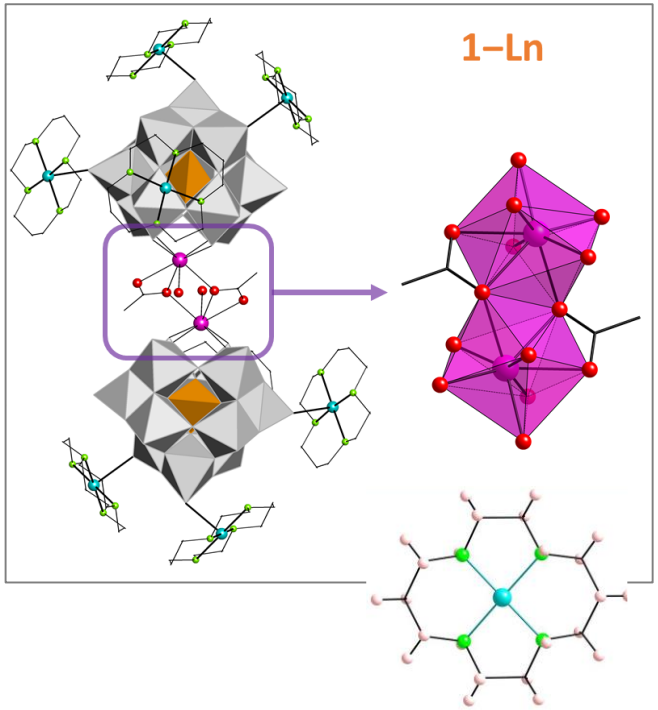

trans–III M(cyclam)}$^{2+}$

FT–IR spectra of **1–Eu** derivative highlighting the bands originating from each subunit.

Jagoba Martín-Caballero et. al. *Inorganic Chemistry* **2019** *58* (7), 4365-4375. DOI: 10.1021/acs.inorgchem.8b03471

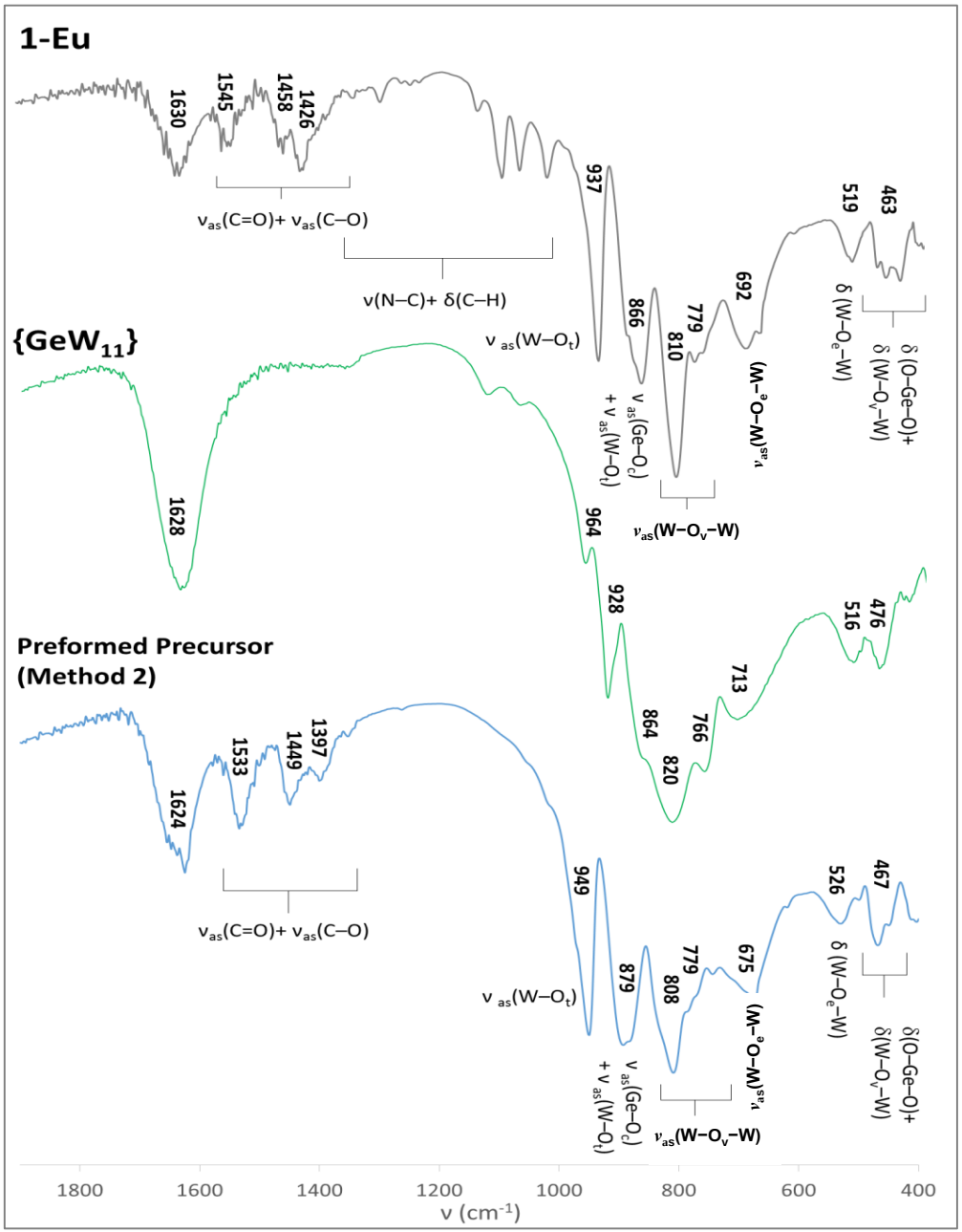

Details of the low–wavenumber region of the FT–IR spectra of **1–Eu** compared to those of the monolacunary {GeW_{11}} and the preformed precursor used.

Structural Analog Comparsion

$Cs_{14}Na_{30}Co^{II}_{6}[\{(GeW_9O_{34})_2Dy^{III}_{3}(\mu_2\text{-}OH)_3(H_2O)_2\}_6\{Co^{II}_{2}Dy^{III}_{3}(\mu_3\text{-}OH)_6(OH_2)_6\}_4]\cdot 370H_2O$

$\{Dy_{30}Co_8\}$

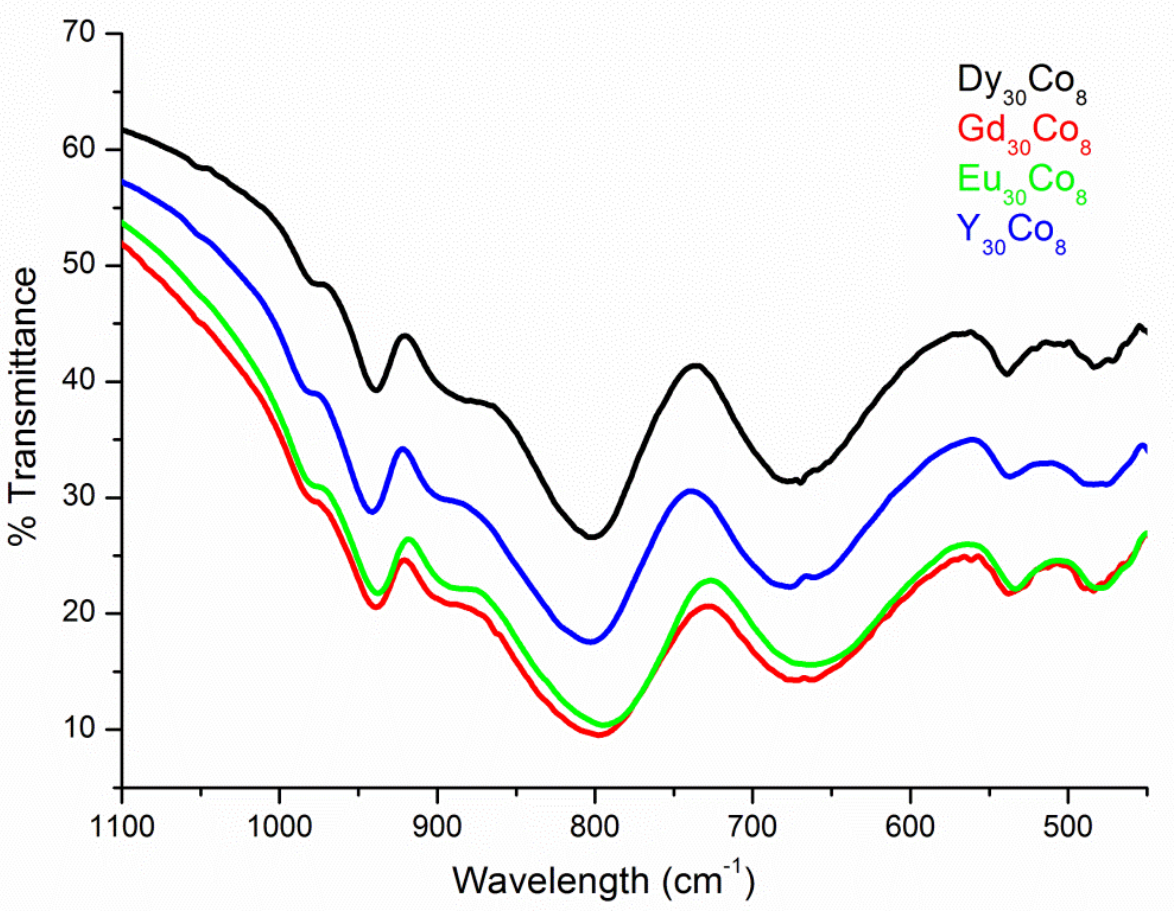

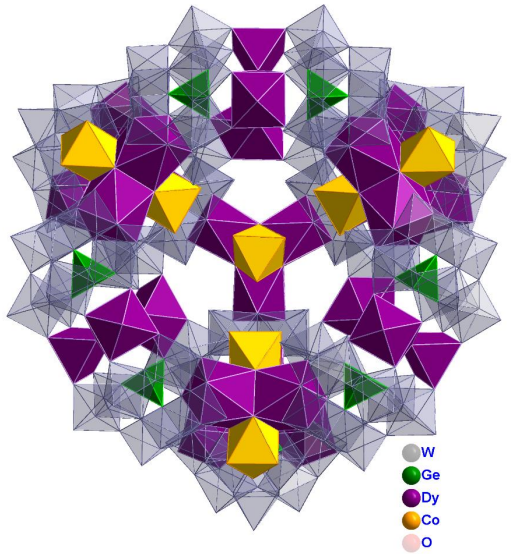

Isolation of Mixtures

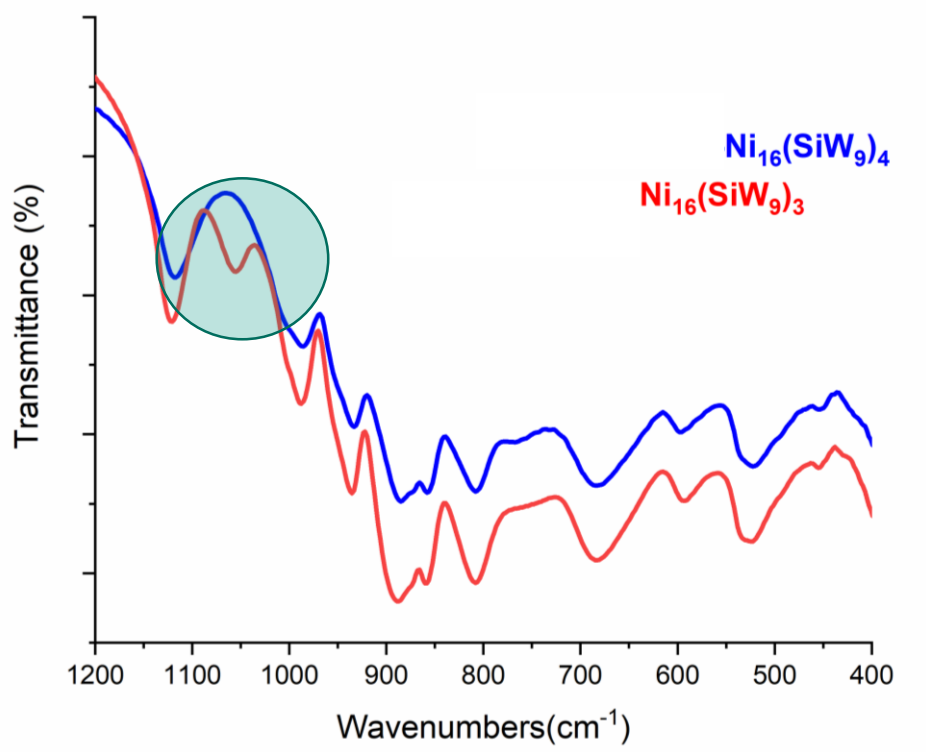

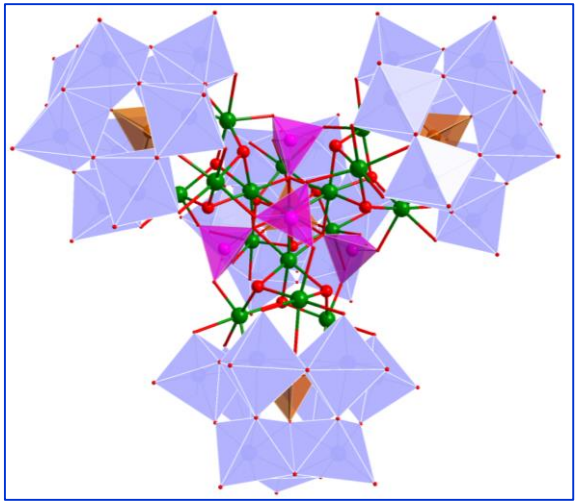

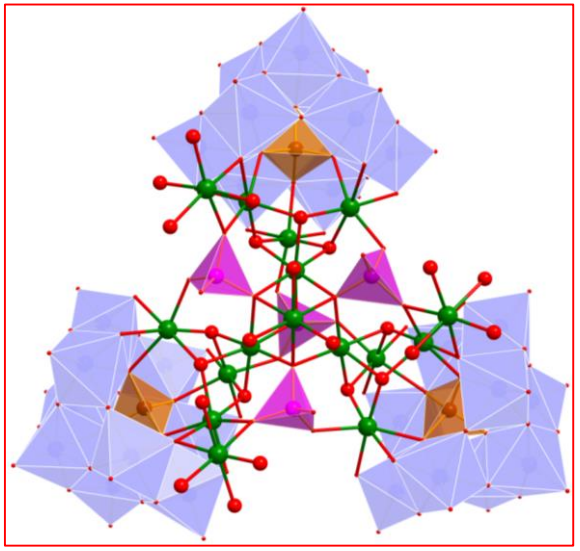

Targetting New Compounds

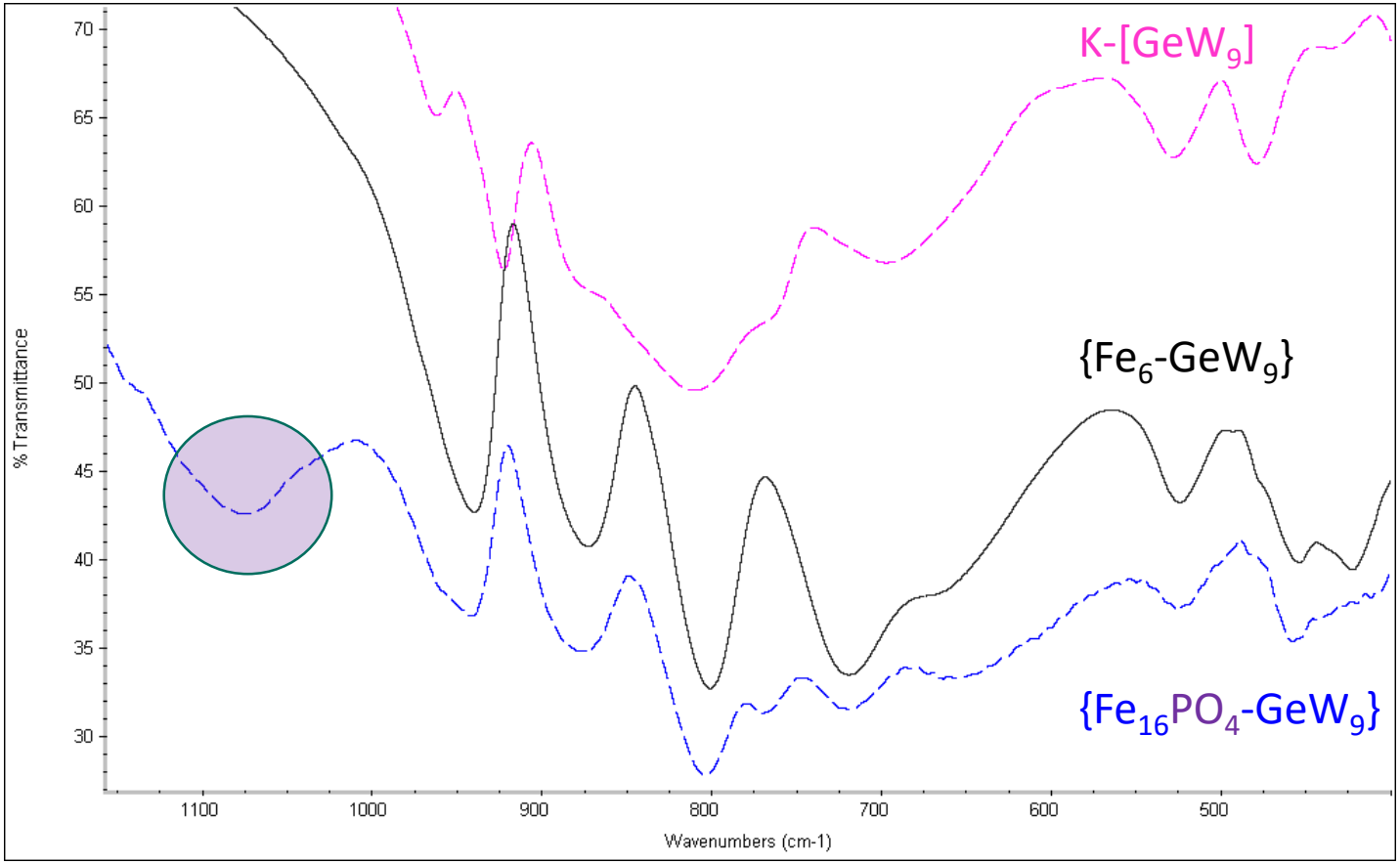

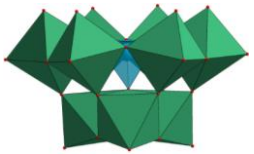

K-[GeW_9]

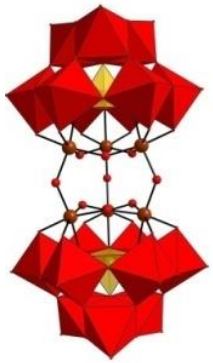

{Fe_6-GeW_9}

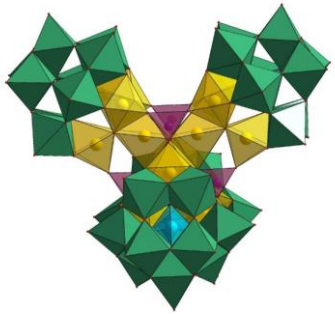

{$Fe_{16}PO_4$-GeW_9}

Powder X-Ray Diffraction (PXRD)

An X-ray diffraction pattern is a plot of the intensity of X-rays scattered at different angles by a sample.

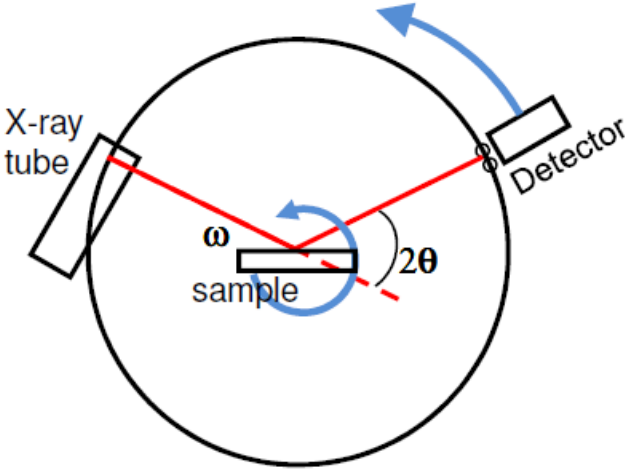

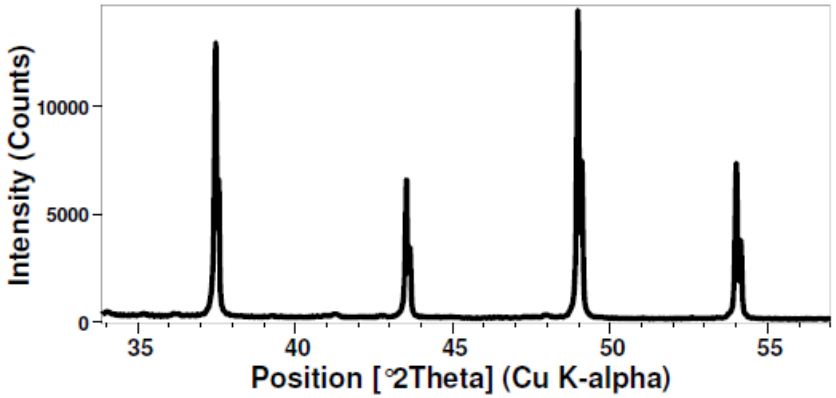

http://prism.mit.edu/xray/

Powder diffractometer

Powder X-Ray Diffraction (PXRD)

Silica (SiO_2) Phases

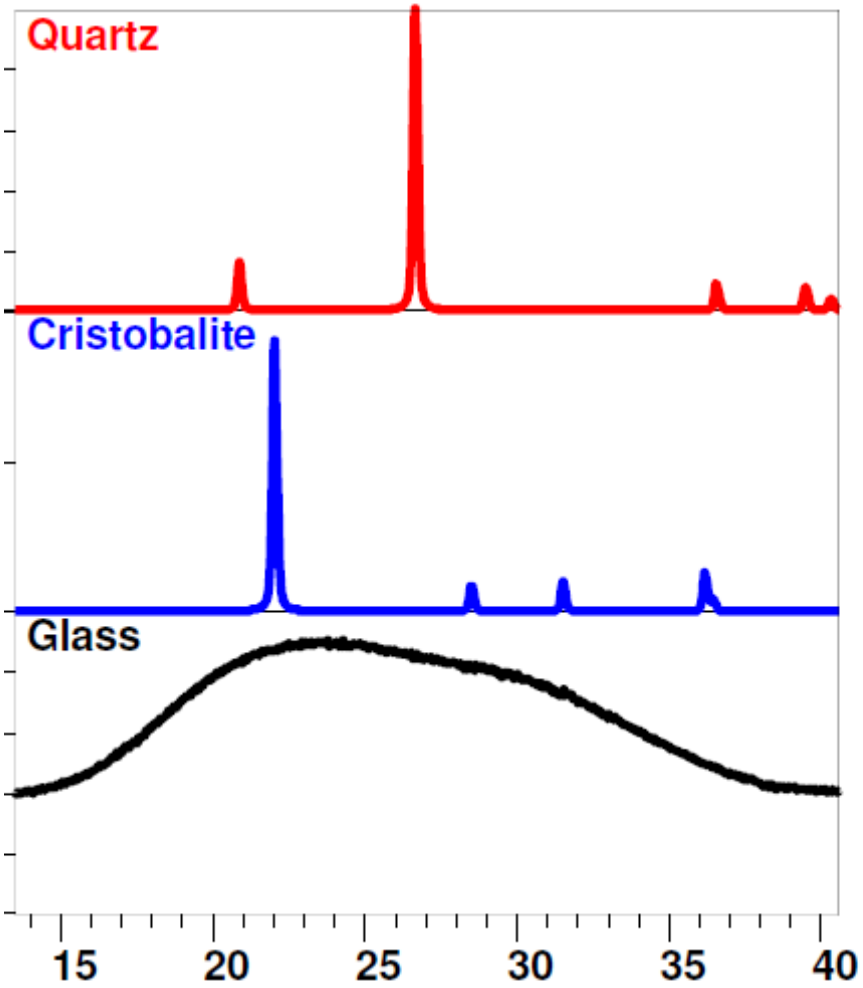

Quartz, cristobalite, and glass are all different phases of SiO_2

– They are chemically identical, but the atoms are arranged differently.

– As shown, the X-ray diffraction pattern is distinct for each different phase.

Powder X-Ray Diffraction (PXRD)

$[Ln(H_2O)_nGeW_{11}O_{39}]^{5-}$ (Ln = Dy (1), Er (2) , *n* = 4,3)

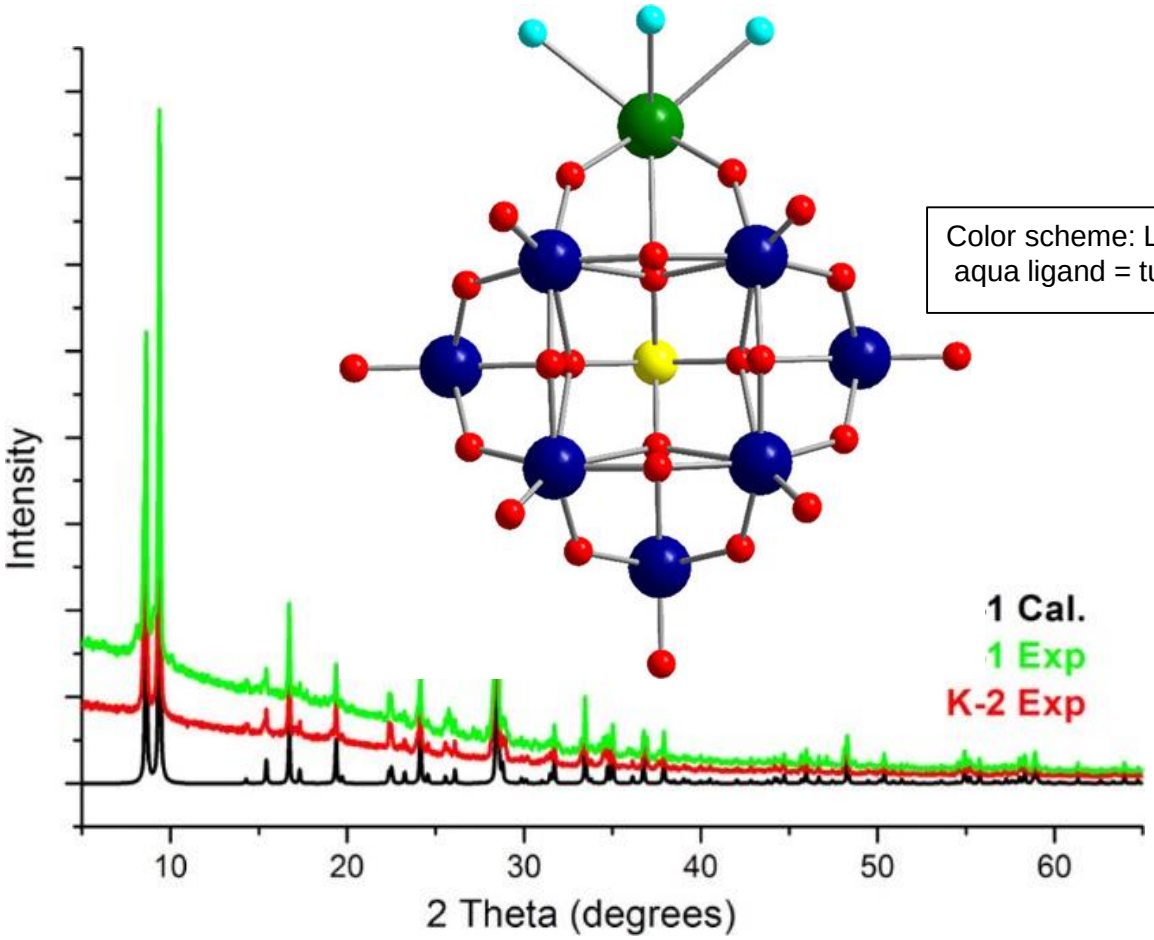

Color scheme: Ln = green; O = red;
aqua ligand = turquoise; W = dark blue, Ge = yellow

Ibrahim, M.; Mbomekallé, I.M.; De Oliveira, P.; Baksi, A.; Carter, A.B.; Peng, Y.; Bergfeldt, T.; Malik, S.; Anson, C.E. *ACS Omega* **2019**, *4*, 21873–21882.

Powder X-Ray Diffraction (PXRD)

$Cs_{14}Na_{30}Co^{II}_{6}[\{(GeW_9O_{34})_2Dy^{III}_{3}(\mu_2\text{-}OH)_3(H_2O)_2\}_6\{Co^{II}_{2}Dy^{III}_{3}(\mu_3\text{-}OH)_6(OH_2)_6\}_4]\cdot\mathbf{370H_2O}$

$\{Dy_{30}Co_8\}$

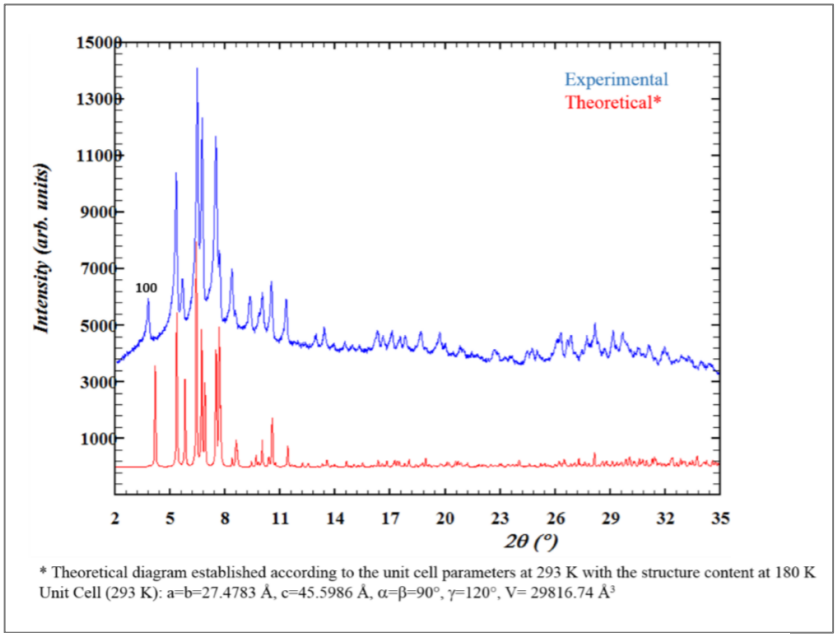

* Theoretical diagram established according to the unit cell parameters at 293 K with the structure content at 180 K
Unit Cell (293 K): a=b=27.4783 Å, c=45.5986 Å, α=β=90°, γ=120°, V= 29816.74 Å³

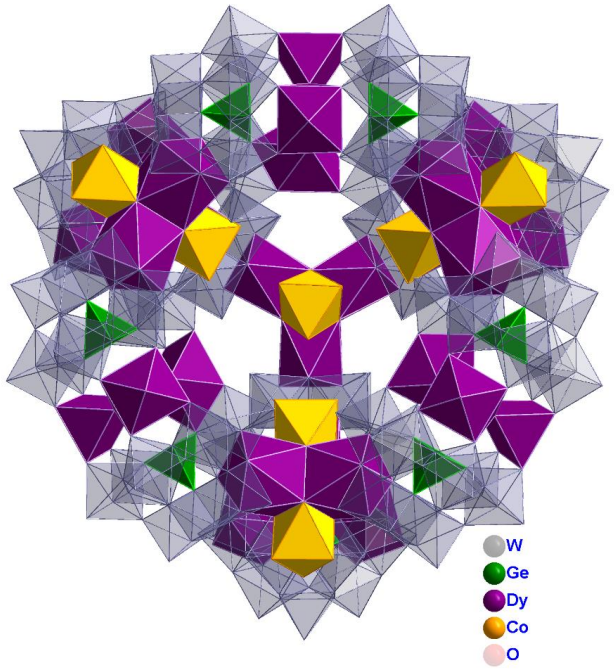

Formula	$Co_{14}Cs_{14}Dy_{30}Ge_{12}H_{842}Na_{30}O_{850}W_{108}$
Formula weight	43426
Crystal System	Trigonal
Space Group	*P*-3
a / Å	29.8349(10)
c / Å	48.184(3)
U / Å^3	37144(4)

Ibrahim, M.; Mereacre, V.; Leblanc, N.; Wernsdorfer, W.; Anson, C.E.; Powell, A.K. *Angew. Chemie - Int. Ed.* **2015**, *54*, 15574–15578.

Thermal Analysis (TA)

Differential thermal analysis (DTA) / Thermogravimetric analysis (TGA)

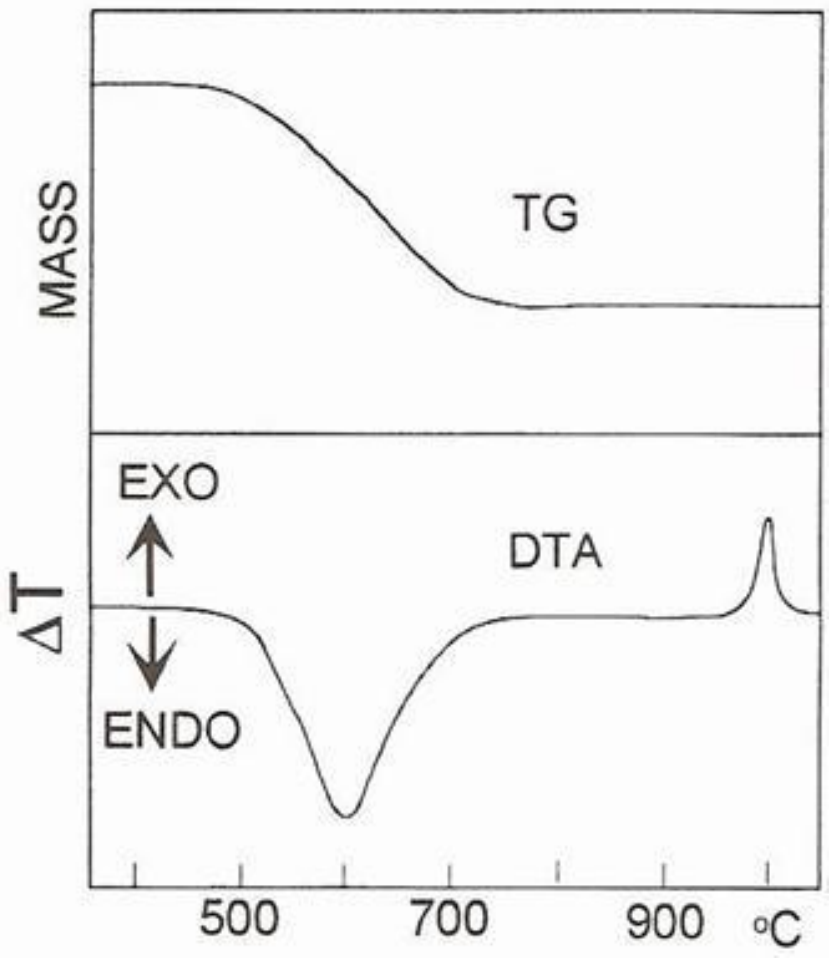

TG measures mass changes in a material as a function of temperature (or time) under a controlled atmosphere. Its principal uses include measurement of a material's thermal stability and composition.

In **DTA**, the temperature of a sample is compared with that of a reference substance, and the liberation or absorption of energy associated with various sample transitions can be correlated with the difference in the two temperature values. Temperature for thermal events such as phase transitions, melting points, crystallization temperatures, and others can be determined.

Thermal Analysis (TA)

Differential thermal analysis (DTA) / Thermogravimetric analysis (TGA)

$K_3Li_8Mn_2[(P_8W_{48}O_{184})(W_4O_{16})K_{10}Li_4Mn_{10}Na(H_2O)_{50}Cl_2]\cdot 62H_2O$

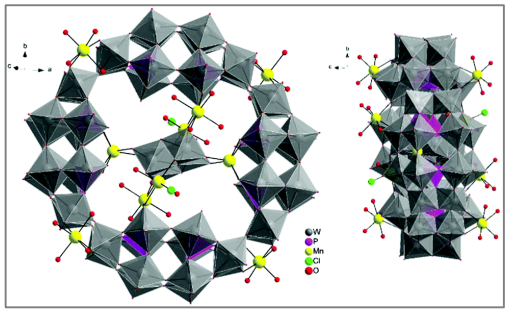

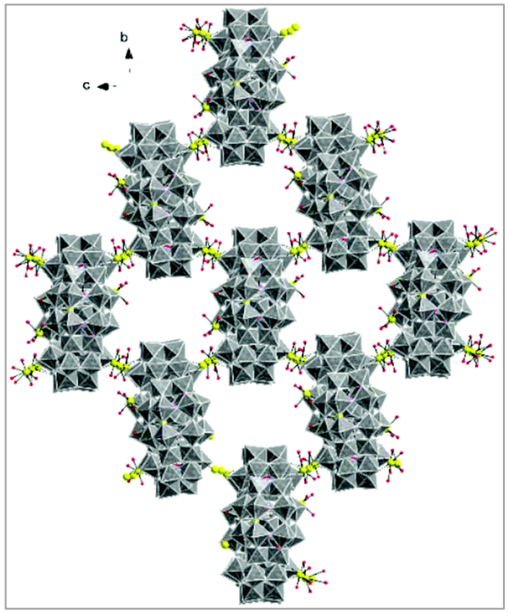

$\leftarrow [(P_8W_{48}O_{184})(W_4O_{16})K_{10}Li_4Mn_{10}Na(H_2O)_{50}Cl_2]^{15-}$

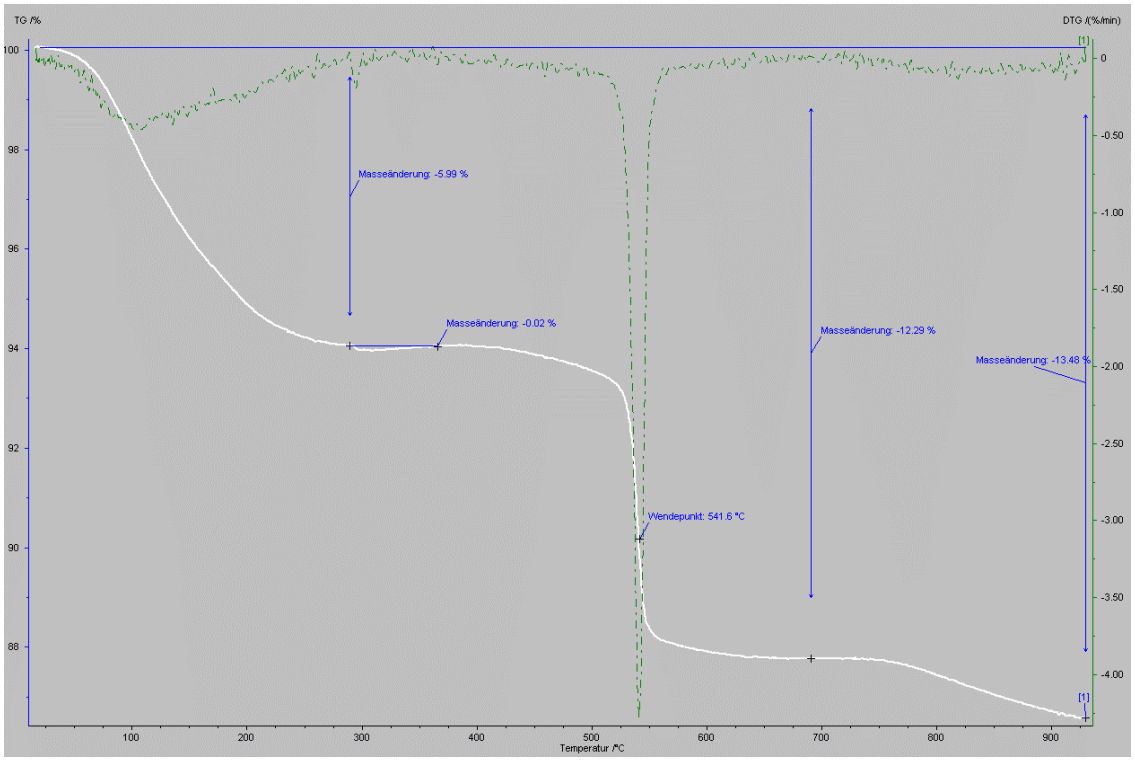

M. Ibrahim, I. M. Mbomekallé, P.deOliveira, G. E. Kostakis, C. E. Anson, *Dalton Trans.* 2019, 48, 15545.

Thermal Analysis (TA)

$Cs_{14}Na_{30}Co^{II}_{6}[\{(GeW_9O_{34})_2Dy^{III}_{3}(\mu_2\text{-}OH)_3(H_2O)_2\}_6\{Co^{II}_{2}Dy^{III}_{3}(\mu_3\text{-}OH)_6(OH_2)_6\}_4]\cdot 370H_2O$

$\{Dy_{30}Co_8\}$

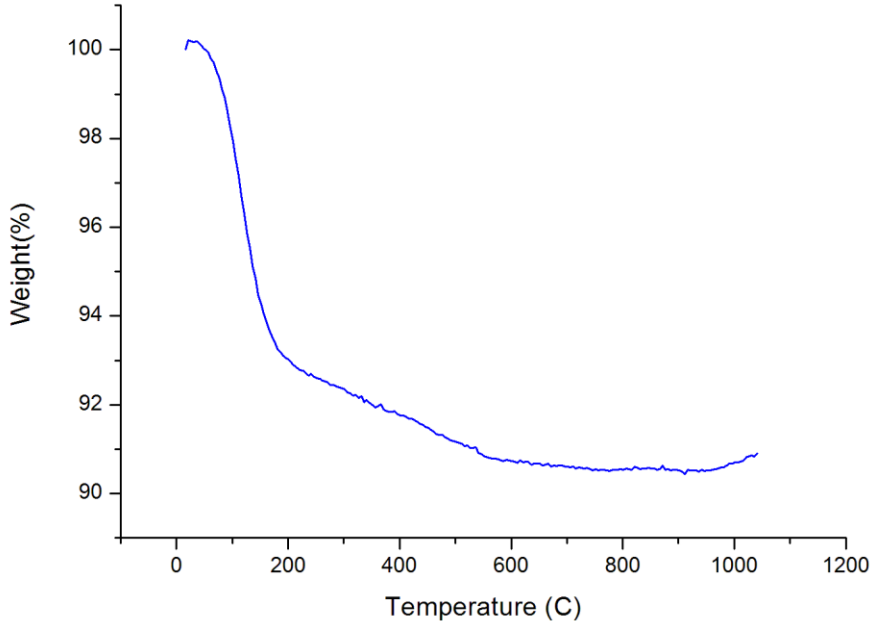

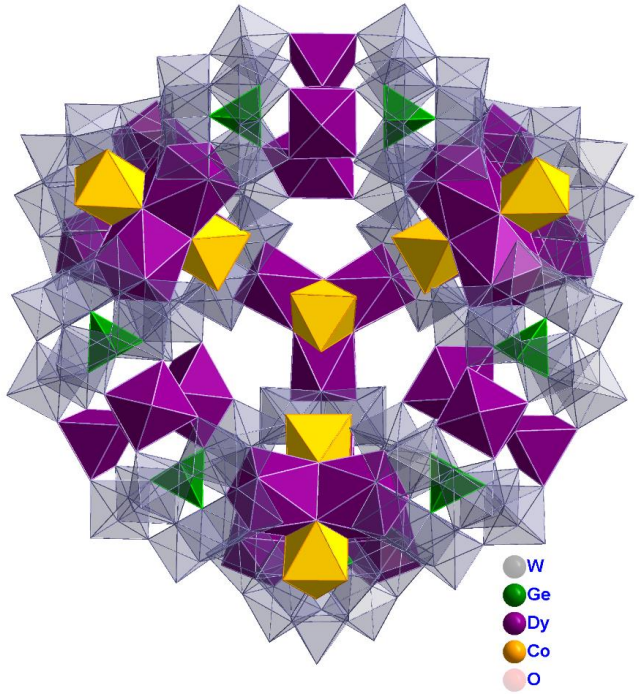

TA methods determine properties—they do not represent a kind of structure analysis.

Thermal Analysis (TA)

$CsNa_{59}[Fe_{32}O_{45}Na_6(OH_2)_{18}(\alpha\text{-}P_2W_{15}O_{56})_6]\cdot ca.260H_2O$

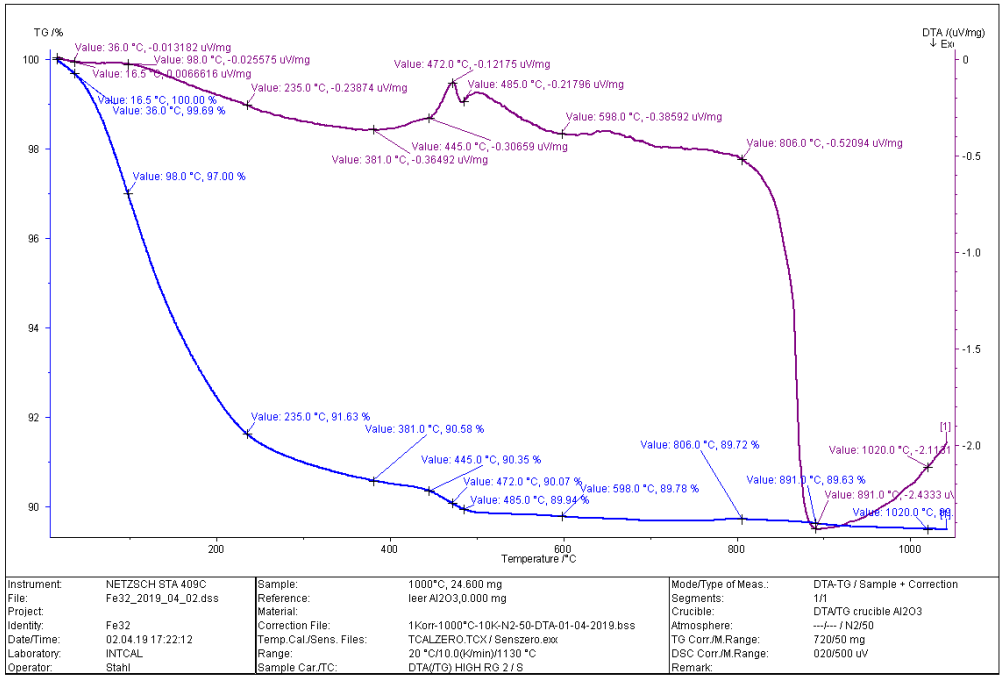

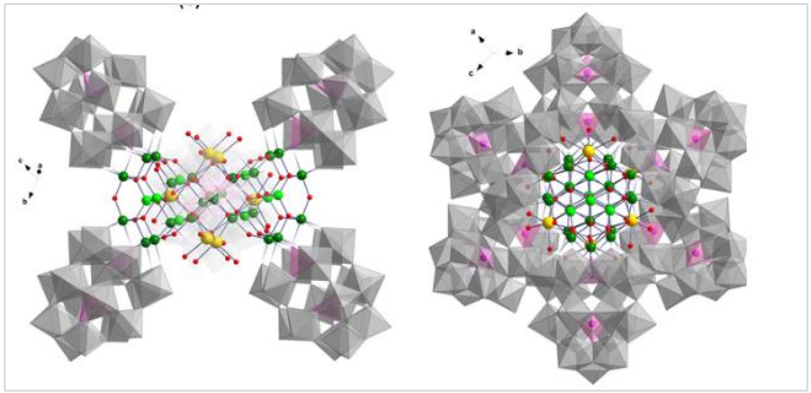

Thermostructural Behavior

$[Cu(cyclam)]_2[\{Cu(cyclam)\}_4\{(\alpha\text{-}GeW_{11}O_{39})Ln(H_2O)(OAc)\}_2]\cdot 18H_2O$ (**1-Ln**, where Ln = La–Lu

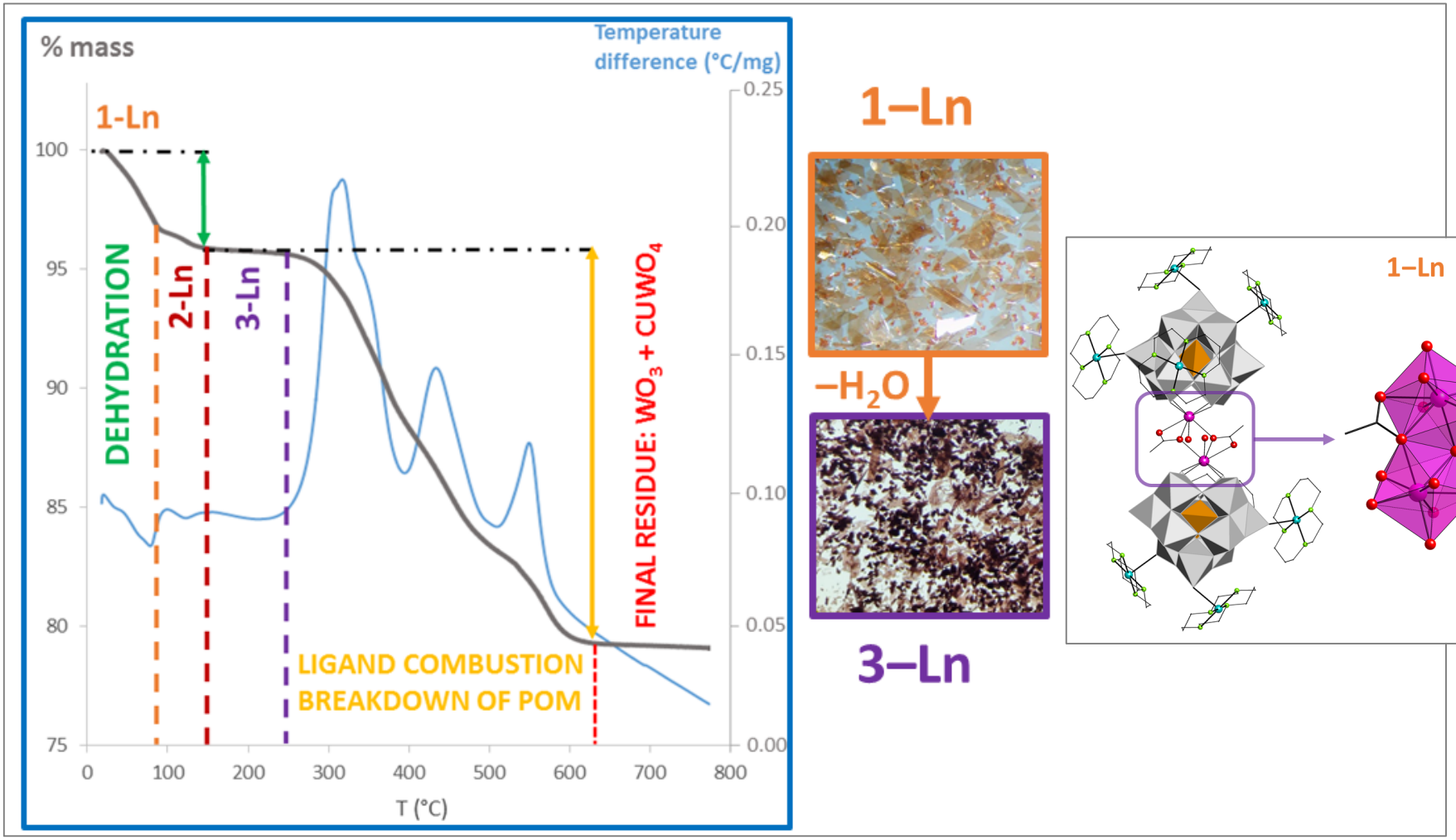

Jagoba Martín-Caballero et. el. *Inorganic Chemistry* **2019** *58* (7), 4365-4375. DOI: 10.1021/acs.inorgchem.8b03471

Thermostructural Behavior

Single–Crystal–to–Single–Crystal Transformations (**SCSC transformations**)

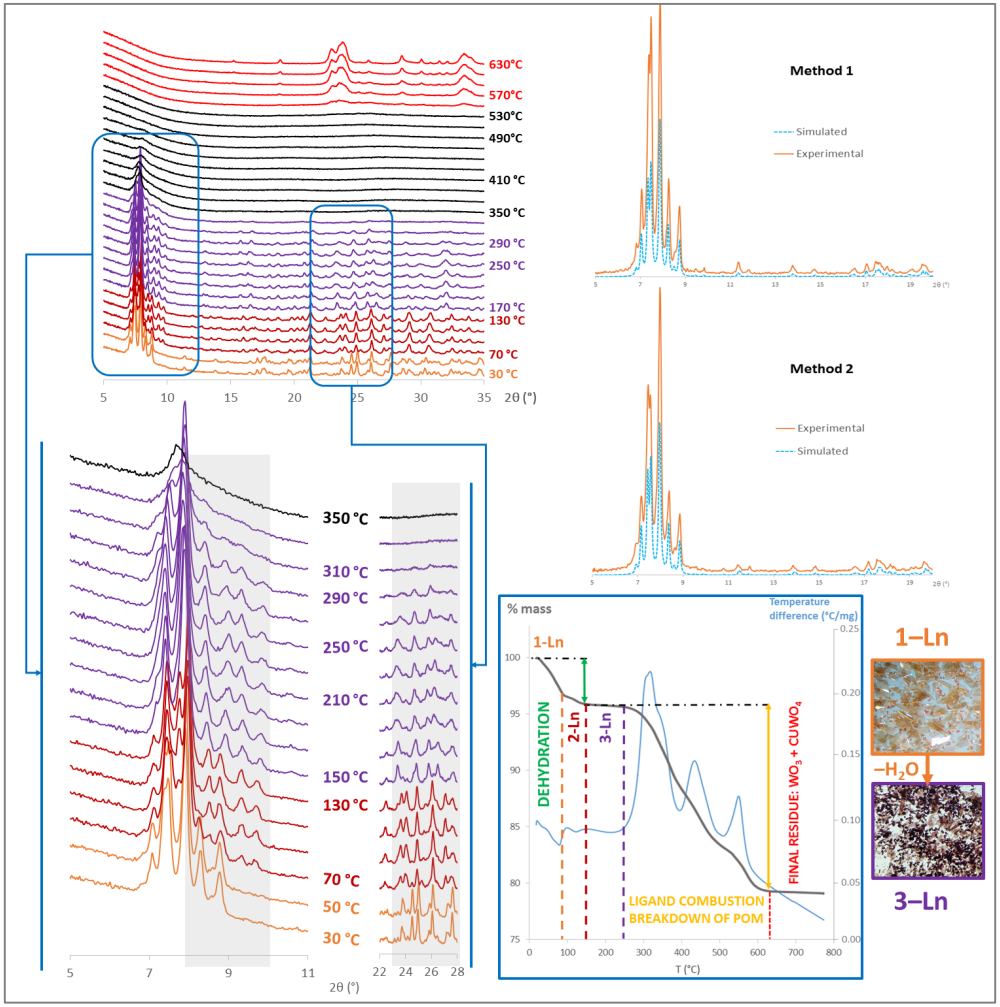

1–Eu $[Cu(cyclam)]_2[\{Cu(cyclam)\}_4\{(\alpha–GeW_{11}O_{39})Eu(H_2O)(\mu–CH_3COO)\}_2]\cdot 17H_2O$

2–Eu $[Cu(cyclam)]_{0.5}[\{Cu(cyclam)\}_{5.5}\{(\alpha–GeW_{11}O_{39})Eu(\mu–CH_3COO)\}_2]\cdot 4H_2O$

3–Eu $[\{Cu(cyclam)\}_6\{(\alpha–GeW_{11}O_{39})Eu(H_2O)(\mu–CH_3COO)\}_2]$

Variable–temperature PXRD patterns (TPXRD) from room temperature to 630 °C of **1–Eu** derivative with details along with the TGA curve and digital photographs of the hydrated and anhydrous phase. Comparison between the xperimental (Method 1 and 2) and simulated PXRD patterns for **1–Eu** are also shown.

Thermostructural Behavior

[{Cu(cyclam)}$(VO_3)_2$]·5H_2O (**1–CuV**)

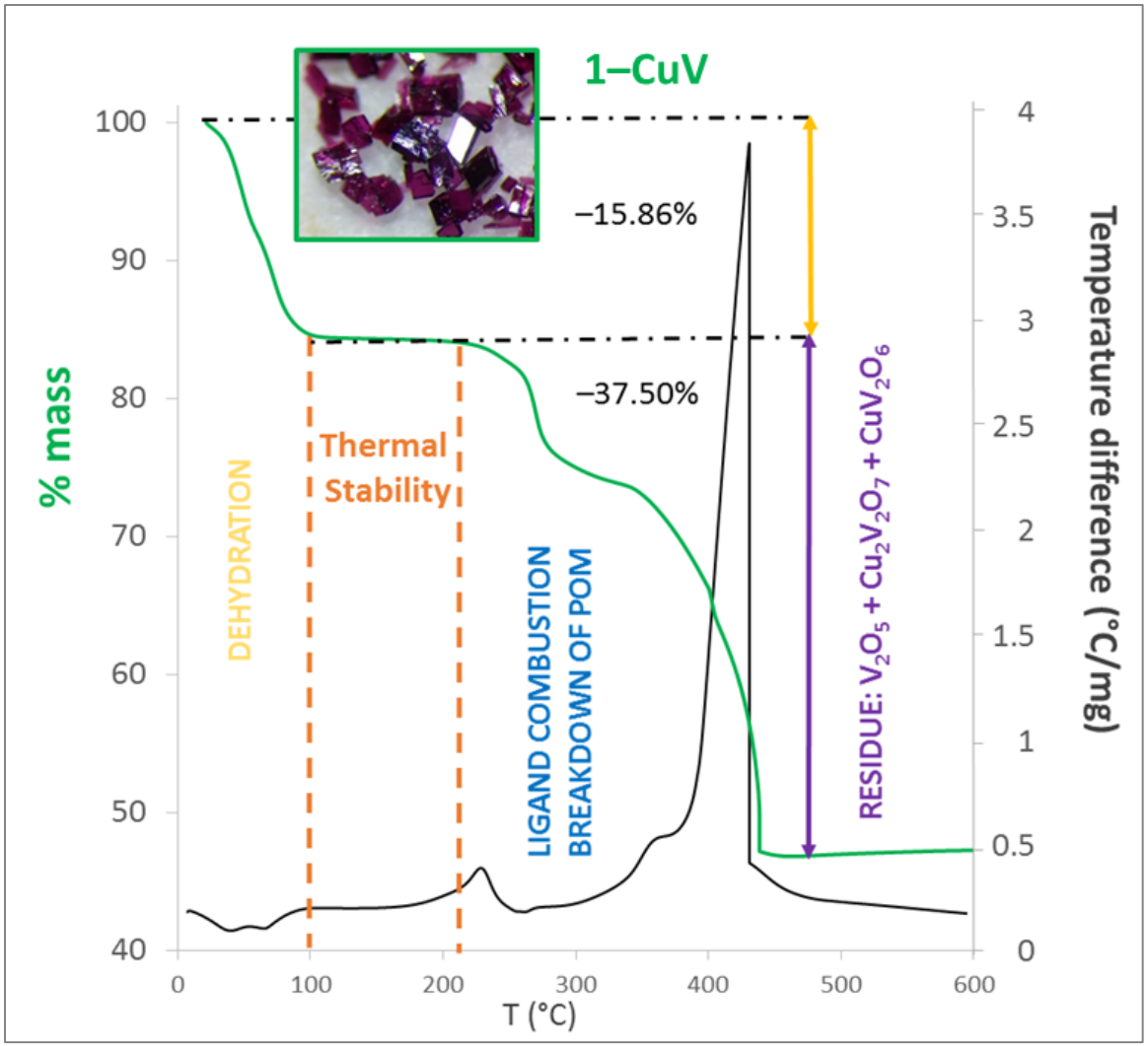

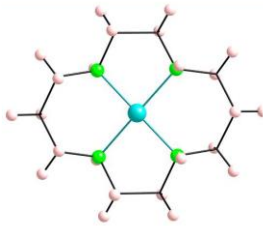

trans–III M(cyclam)$\}^{2+}$

Martín-Caballero *et.al.* *Inorg. Chem.* **2016**, *55*, 4970– 4979, DOI: 10.1021/acs.inorgchem.6b00505

Thermostructural Behavior

Scheme of the reversibility of the SCSC transformations between **1–4–CuV**

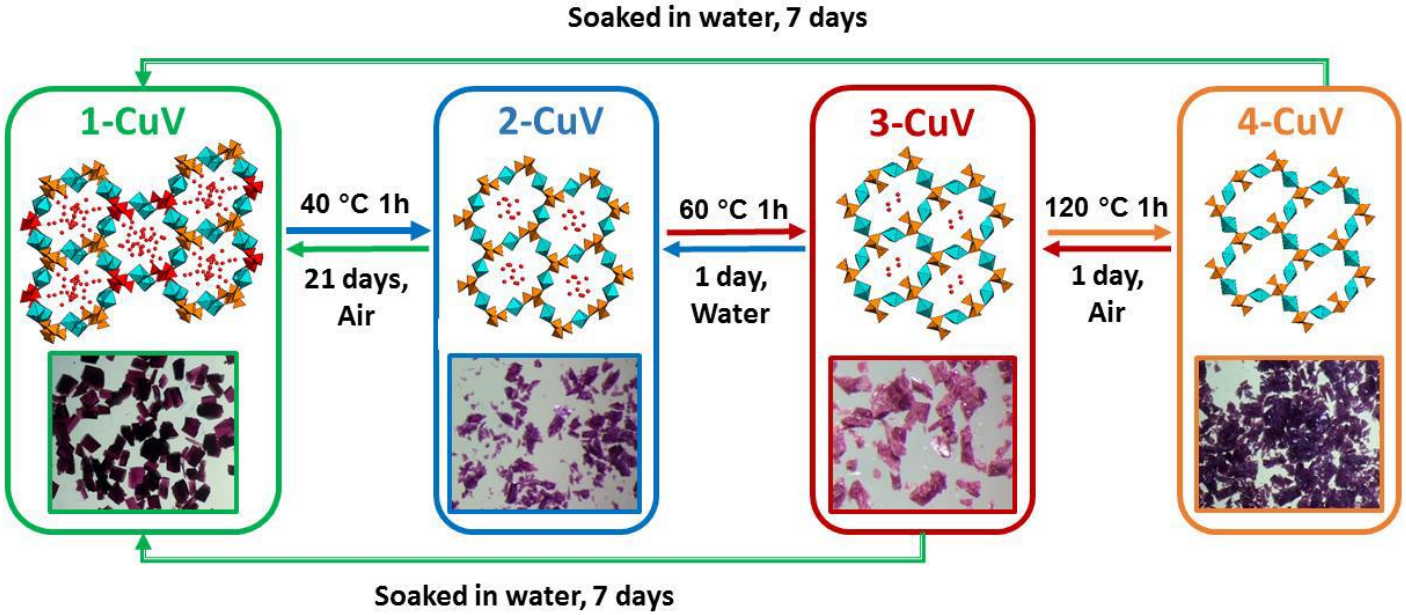

[{Cu(cyclam)}$(VO_3)_2$]·3H_2O (2–CuV). Single crystals of **[{Cu(cyclam)}$(VO_3)_2$]·5H_2O (1–CuV)** were heated at 40 °C in an oven for 1 h, which produced a color change from dark purple to light purple.

[{Cu(cyclam)}$(VO_3)_2$]·1.3H_2O (3–CuV). Single crystals of **1–CuV** were heated in an oven at 60 °C for 1 h, with their color changing to dark pink.

[{Cu(cyclam)}$(VO_3)_2$] (4–CuV). Single crystals of **1–CuV** were heated in an oven at 120 °C for 1 h and a slight color change to darker purple was observed.

Thermostructural Behavior

Single–Crystal–to–Single–Crystal Transformations (**SCSC transformations**)

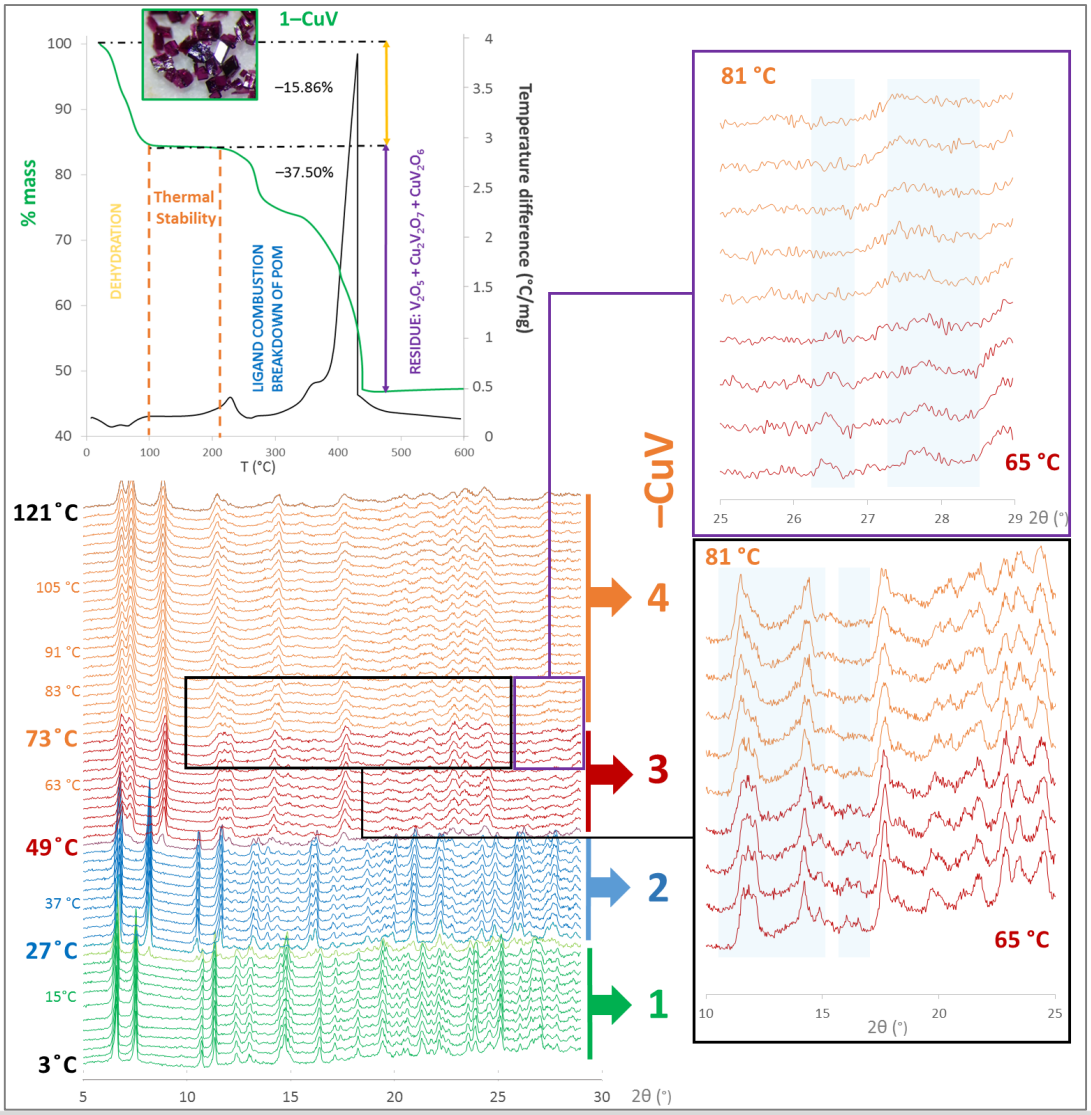

1–CuV $[\{Cu(cyclam)\}(VO_3)_2]\cdot 5H_2O$
2–CuV $[\{Cu(cyclam)\}(VO_3)_2]\cdot 3H_2O$
3–CuV $[\{Cu(cyclam)\}(VO_3)_2]\cdot 1.3H_2O$
4–CuV $[\{Cu(cyclam)\}(VO_3)_2]$

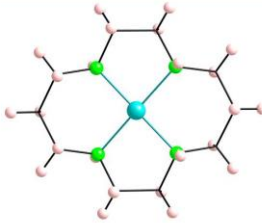

trans–III M(cyclam)}$^{2+}$

Elemental Analysis

Inductively Coupled Plasma-Optical Emission Spectrometry (ICP-OES)

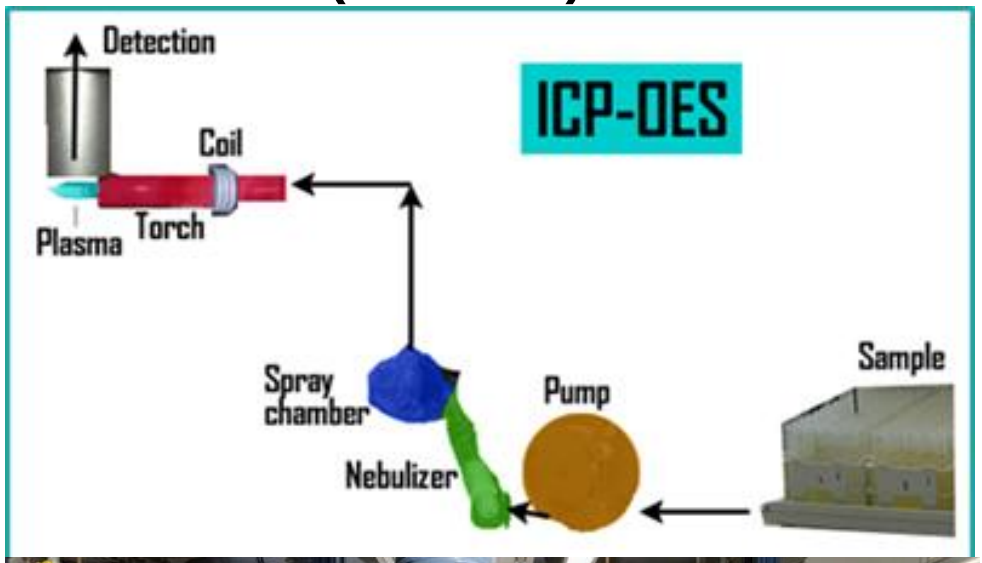

Elemental Analysis

Inductively Coupled Plasma Mass Spectrometry (ICP-MS)

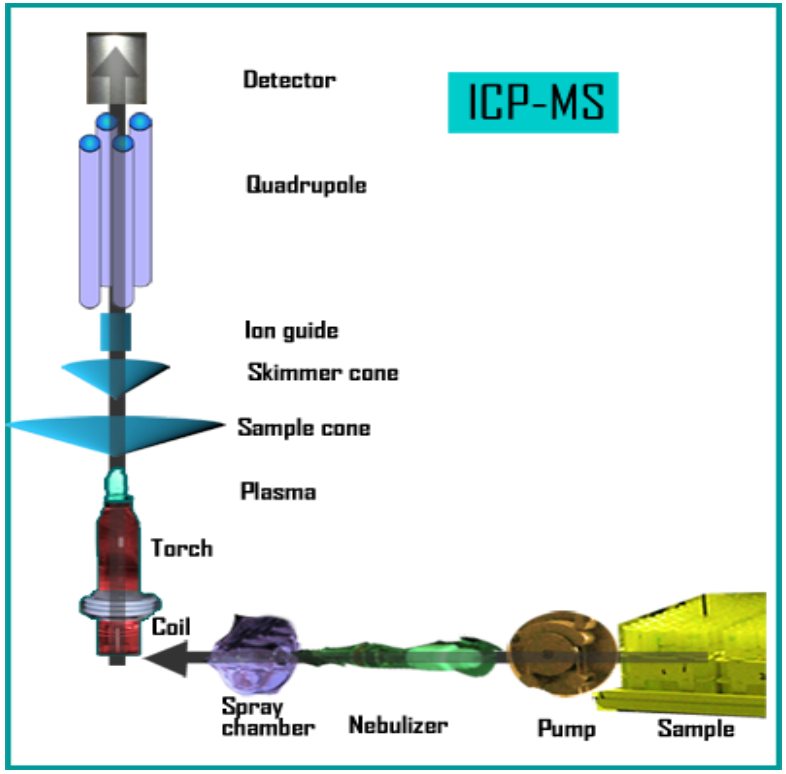

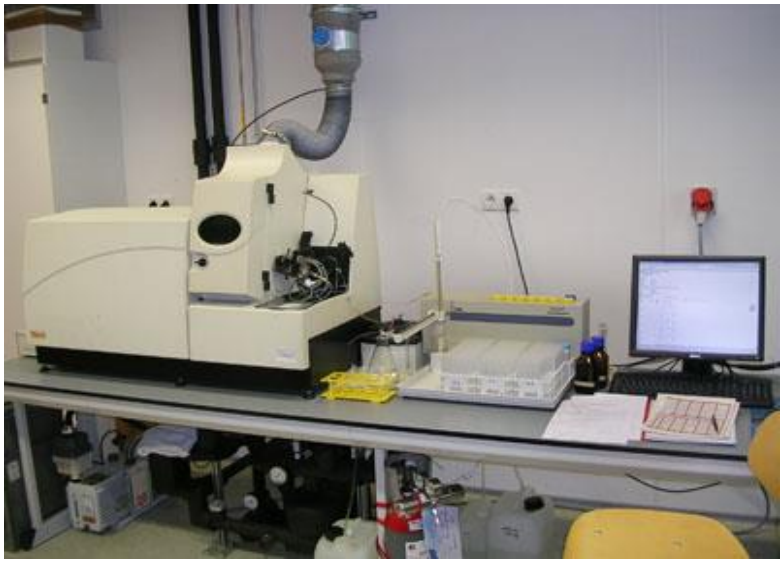

Elemental Analysis

Elemental analysis (%) for $Na_{22}Rb_6[\{Co_4(OH)_3PO_4\}_4(A\text{-}\alpha\text{-}PW_9O_{34})_4]\cdot 76\,H_2O$:

Calcd: Na 3.94, Rb 4.00, P 1.93, Co 7.35, W 51.57
Found: Na 3.16, Rb 4.14, P 1.95, Co 7.15, W 51.30

Elemental analysis (%) for $Cs_{14}Co_6Na_{30}$
$[\{(GeW_9O_{34})_2Dy^{III}{}_3(\mu_2\text{-}OH)_3(H_2O)_2\}_6\{Co^{II}{}_2Dy^{III}{}_3(\mu_3\text{-}OH)_6(OH_2)_6\}_4]\cdot$ca. 370 H_2O

Calcd: Cs 4.28, Na 1.58, Co 1.90, W 45.72, Ge 2.01, Dy 11.22
Found: Cs 4.13, Na 1.46, Co 1.86, W 45.80, Ge 1.94, Dy 11.50

Electronic Spectroscopy

The addenda ions in POMs have d^0 electronic configuration, and as a result, only one absorption band occurs in the UV-vis between 190 and 400 nm due to the oxygen-to-metal charge transfer transition: **p_π–d_π charge-transfer transitions** of the $O_t \rightarrow W^{VI}$ (O_t – terminal oxygen atom), and p_π–d_π charge-transfer transitions of the $O_{b,c} \rightarrow W^{VI}$ ($O_{b,c}$ – bridge oxygen atoms) (

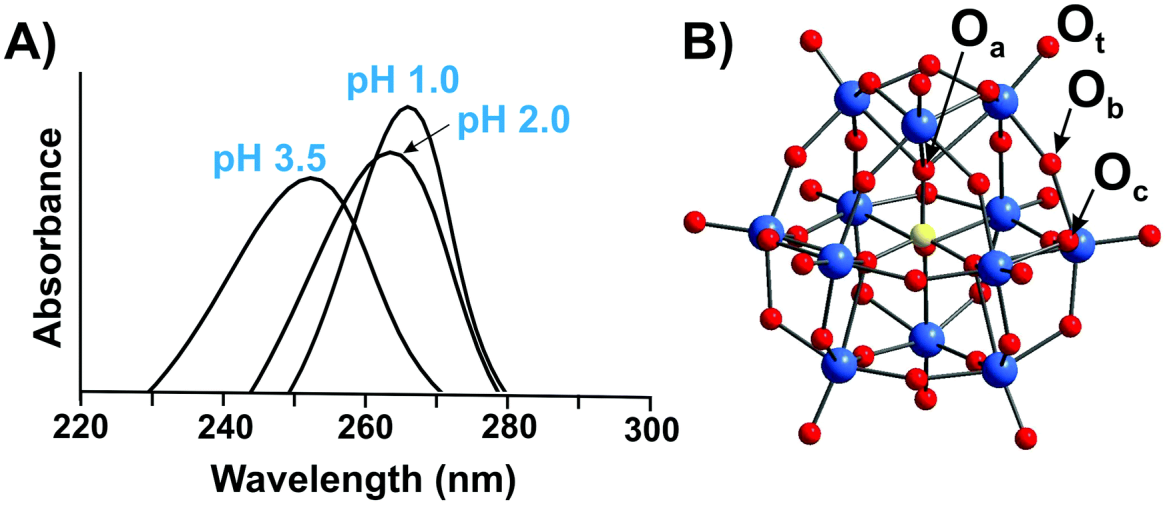

(A) UV-vis spectra of aqueous solutions of $H_3[P^VW^{VI}_{12}O_{40}]$ recorded at pH 1.0; 2.0 and 3.5.
The decomposition of Keggin anion can be clearly seen already at pH 3.5 by shifting of the maximum absorption from 263 nm to 252.5 nm. (B) $[P^VW^{VI}_{12}O_{40}]^{3-}$ with the indicated types of oxygen atoms: μ_3-O_a – oxygen atom connected to heteroatom P^V; μ_2-O_b and μ_2-O_c – two types of bridging atoms in the structure; O_t – terminal oxygen atom.

N. I. Gumerova and A. Rompel , *Chem. Soc. Rev.*, 2020, 49 , 7568 —7601

Mass Spectrometry (MS)

Electrospray-ionization mass-spectrometry (ESI-MS) is suitable for the elucidation of solution phase equilibria of stable upon ionization anions, since it enables semi-quantitative detection of both cationic and anionic species in aqueous solvents with excellent detection limits. POMs are ideal candidates for mass-spectrometry studies since they exhibit complex isotopic envelopes resulting from the high number of stable isotopes as for tungsten **(^{182}W, 26.5%; ^{183}W, 14.3%; ^{184}W, 30.6%; ^{186}W, 28.4%) or molybdenum (^{92}Mo, 14.8%; ^{94}Mo, 9.3%; ^{95}Mo, 15.9%; ^{96}Mo, 16.7%; ^{97}Mo, 9.6%; ^{98}Mo, 24.1%; ^{100}Mo, 9.6%),** and are **intrinsically charged.**

H. N. Miras, E. F. Wilson and L. Cronin, *Chem. Commun*., 2009, 1297–1311
N. I. Gumerova and A. Rompel , *Chem. Soc. Rev.*, 2020, 49 , 7568 —7601

Mass Spectrometry (MS)

$[\{Er(H_2O)(CH_3COO)(P_2W_{17}O_{61})\}_2]^{16-}$

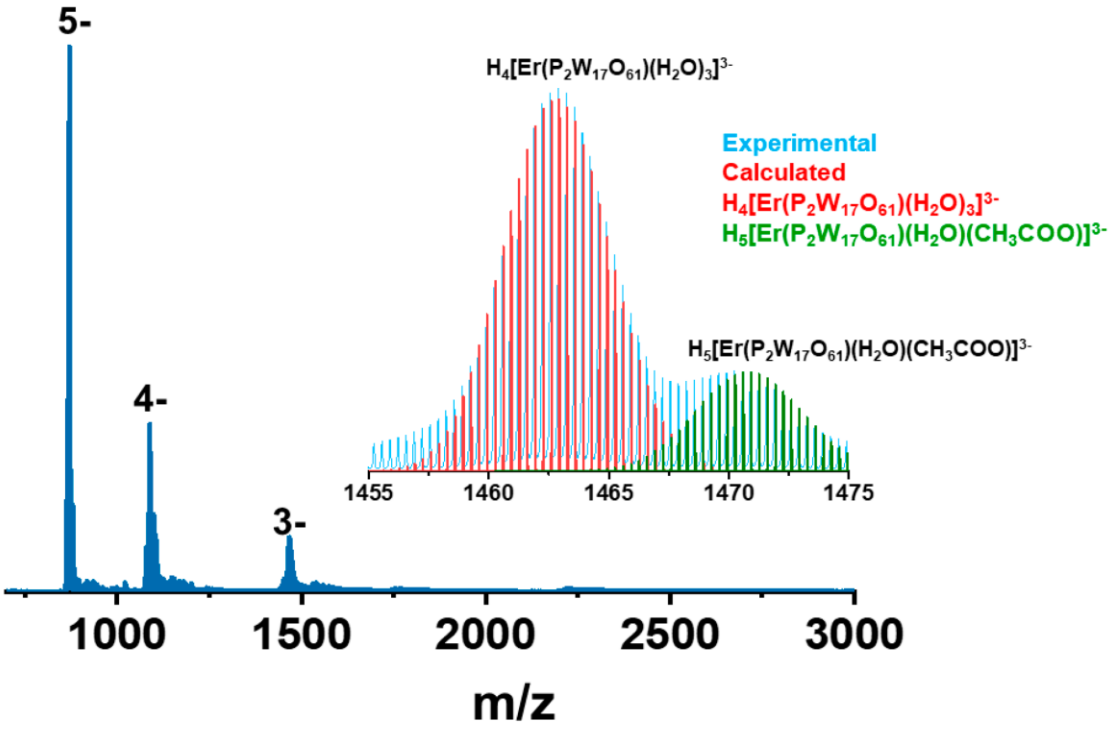

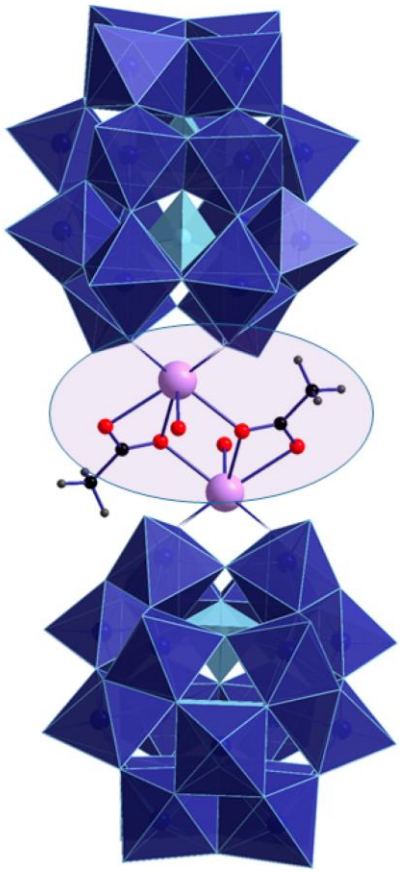

Negative ion ESI MS in a water/ACN mixture. The 3- region is expanded in the inset and two peaks are compared with their calculated isotope pattern.

M. Ibrahim, A. Baksi, Y. Peng, F.K. Al-Zeidaneen, I.M. Mbomekallé, P. de Oliveira, C.E. Anson, *Molecules* 2020, *25*, 4229.

Mass Spectrometry (MS)

$K_5[Dy(H_2O)_4GeW_{11}O_{39}]\cdot 16H_2O$

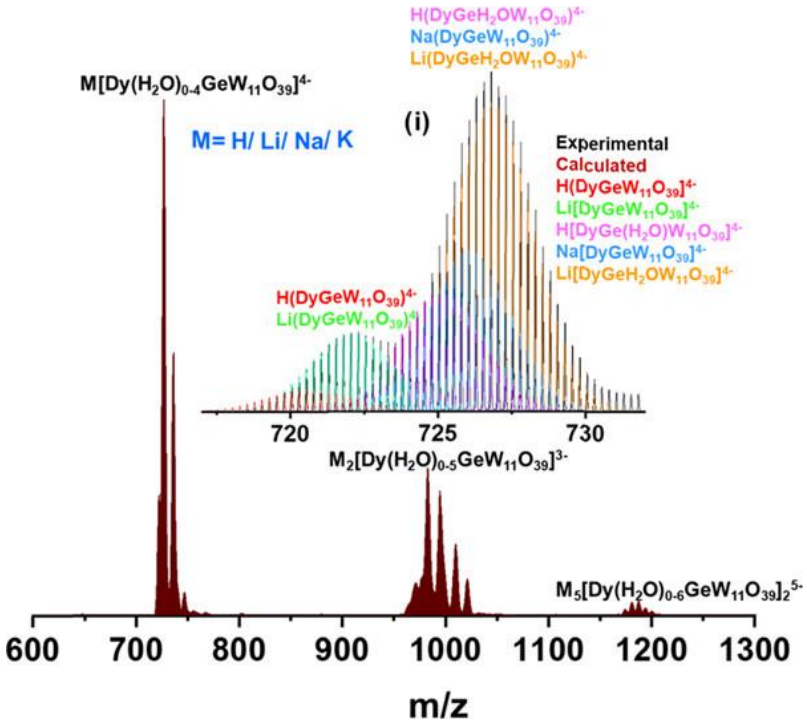

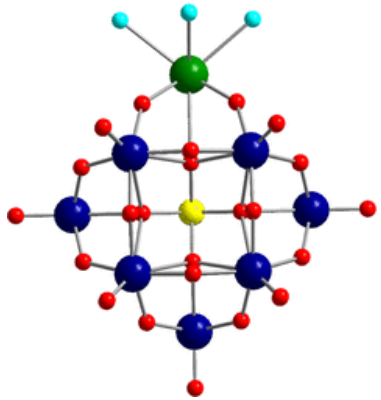

The crystal packing arrangement

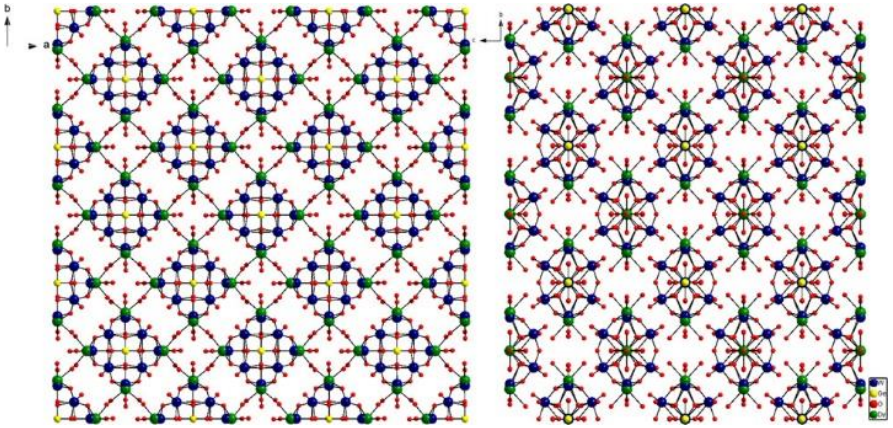

ESI MS: 2 sets of peaks at the mass range 710–760 and 960–1030 corresponding to 4- and 3-charge state, respectively. Strongest peak at *m/z* 715–730 is expanded in the inset (i). Different alkali-metal-exchanged peaks were observed and the mass envelope is compared with 5 different possible compositions, and their calculated isotope distribution pattern is overlaid.

M. Ibrahim, I. M. Mbomekallé, P. de Oliveira, A. Baksi, A. B. Carter, Y. Peng, T. Bergfeldt, S. Malik, C.E. Anson,. ACS Omega 2019, 4, 21873–21882

Multinuclear Magnetic Resonance (NMR)

Nuclear magnetic resonance spectroscopy has been carried out on POMs containing NMR-active nuclei, i.e.^{31}P (natural abundance (NA): NA (**^{31}P**) = 100%; nuclear spin (I): I = 1/2), **^{51}V** (NA = 99.75%; I = 7/2), **^{17}O** (NA = 0.04%; I = 5/2), ^{1}H (NA = 99.98%; I = 1/2), **^{29}Si** (NA = 4.7%; 1/2), and, later, **^{95}Mo** (NA = 15.87%; I = 5/2) and **^{183}W** (NA = 14.32%, I = 1/2), to investigate their solution structures and dynamics since the 1970s. For reliable identification of a POM species in solution, it is desirable, whenever possible, to measure NMR spectra of all NMR-active core components.

And ^{19}F, ^{77}Se, ^{119}Sn, ^{195}Pt,…..

N. I. Gumerova and A. Rompel , *Chem. Soc. Rev.*, 2020, 49 , 7568 —7601

Multinuclear Magnetic Resonance (NMR)

^{19}F, ^{31}P, ^{77}Se, ^{119}Sn, ^{195}Pt,^{183}W…..

^{27}Aluminium	(^{2}Hydrogen)	(^{41}Potassium)
^{39}Argon	*^{3}Hydrogen*	^{1}Proton
^{75}Arsenic	(^{113}Indium)	^{103}Rhodium
^{135}Barium	^{115}Indium	(^{85}Rubidium)
^{137}Barium	^{127}Iodine	^{87}Rubidium
^{9}Beryllium	^{57}Iron	*^{45}Scandium*
^{209}Bismuth	*^{83}Krypton*	^{77}Selenium
(^{10}Boron)	(^{138}Lanthanum)	^{29}Silicon
^{11}Boron	^{139}Lanthanum	^{107}Silver
(^{79}Bromine)	^{207}Lead	^{109}Silver
^{81}Bromine	^{6}Lithium	^{23}Sodium
(^{111}Cadmium)	^{7}Lithium	^{87}Strontium
^{113}Cadmium	^{25}Magnesium	^{33}Sulfur
^{43}Calcium	^{55}Manganese	(^{123}Tellurium)
^{13}Carbon	^{199}Mercury	^{125}Tellurium
^{133}Cesium	*^{201}Mercury*	(^{115}Tin)
^{35}Chlorine	^{95}Molybdenum	(^{117}Tin)
^{37}Chlorine	(^{97}Molybdenum)	^{119}Tin
^{53}Chromium	*^{21}Neon*	(^{47}Titanium)
^{63}Copper	^{61}Nickel	^{49}Titanium
^{65}Copper	^{14}Nitrogen	*^{3}Tritium*
^{59}Cobalt	^{15}Nitrogen	^{183}Tungsten
(^{2}Deuterium)	*^{187}Osmium*	*^{235}Uranium*
^{19}Fluorine	^{189}Osmium	(^{50}Vanadium)
(^{69}Gallium)	^{17}Oxygen	^{51}Vanadium
^{71}Gallium	^{31}Phosphorus	^{129}Xenon
^{73}Germanium	^{195}Platinum	(^{131}Xenon)
^{3}Helium	^{39}Potassium	^{67}Zinc
^{1}Hydrogen	^{40}Potassium	

http://chem.ch.huji.ac.il/nmr/techniques/1d/multi.html

Multinuclear Magnetic Resonance (NMR)

Properties of ^{31}P

Property	Value
Spin	½
Natural abundance	100%
Chemical shift range	430 ppm, from -180 to 250
Frequency ratio (Ξ)	40.480742%
Reference compound	85% H_3PO_4 in H_2O = 0 ppm
Linewidth of reference	1 Hz
T_1 of reference	0.5 s
Receptivity rel. to ^{1}H at natural abundance	6.63×10^{-3}
Receptivity rel. to ^{1}H when enriched	6.63×10^{-3}
Receptivity rel. to ^{13}C at natural abundance	37.7
Receptivity rel. to ^{13}C when enriched	37.7

Multinuclear Magnetic Resonance (NMR)

Properties of ^{77}Se

Property	Value
Spin	1/2
Natural abundance	7.63%
Chemical shift range	3000 ppm, from -1000 to 2000
Frequency ratio (Ξ)	19.071513%
Reference compound	Me_2Se
Linewidth of reference	~0.5 Hz
T_1 of reference	~30 s
Receptivity rel. to ^{1}H at natural abundance	5.37×10^{-4}
Receptivity rel. to ^{1}H when enriched	7.04×10^{-3}
Receptivity rel. to ^{13}C at natural abundance	3.15
Receptivity rel. to ^{13}C when enriched	41.3

Multinuclear Magnetic Resonance (NMR)

Properties of ^{51}V

Property	Value
Spin	7/2
Natural abundance	99.750%
Chemical shift range	1900 ppm, from -1900 to 0
Frequency ratio (Ξ)	26.302948%
Reference compound	$VOCl_3$ (90%) in C_6D_6
Linewidth of reference	21 Hz
T_1 of reference	0.0203 s
Receptivity rel. to ^{1}H at natural abundance	0.383
Receptivity rel. to ^{1}H when enriched	0.384
Receptivity rel. to ^{13}C at natural abundance	2250
Receptivity rel. to ^{13}C when enriched	2256

Multinuclear Magnetic Resonance (NMR)

Properties of ^{27}Al

Property	Value
Spin	5/2
Natural abundance	100%
Chemical shift range	400 ppm, from -200 to 200
Frequency ratio (Ξ)	26.056859%
Reference compound	1.1 m $Al(NO_3)_3$ in D_2O
Linewidth of reference	11 Hz
T_1 of reference	0.03 s
Receptivity rel. to ^{1}H at natural abundance	0.207
Receptivity rel. to ^{1}H when enriched	0.207
Receptivity rel. to ^{13}C at natural abundance	1220
Receptivity rel. to ^{13}C when enriched	1220

Chemical shift ranges for ^{27}Al NMR

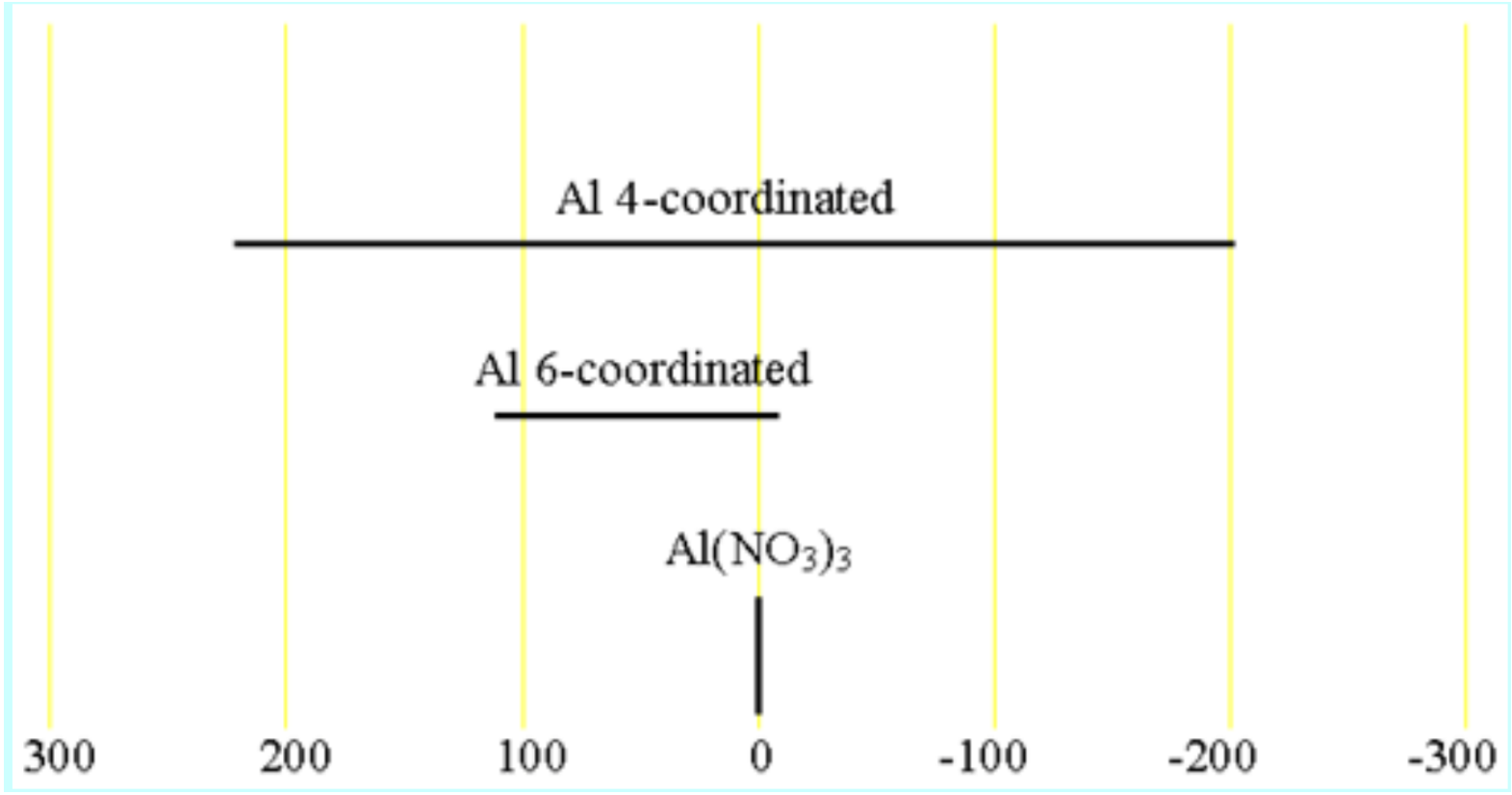

Multinuclear Magnetic Resonance (NMR)

Properties of ^{17}O

Property	Value
Spin	5/2
Natural abundance	0.038%
Chemical shift range	1160 ppm, from -40 to 1120
Frequency ratio (Ξ)	13.556457%
Reference compound	D_2O
Linewidth of reference	69 Hz
T_1 of reference	0.02 s
Receptivity rel. to ^{1}H at natural abundance	1.11×10^{-5}
Receptivity rel. to ^{1}H when enriched	0.0291
Receptivity rel. to ^{13}C at natural abundance	0.0650
Receptivity rel. to ^{13}C when enriched	171

Chemical shift ranges for ^{17}O NMR

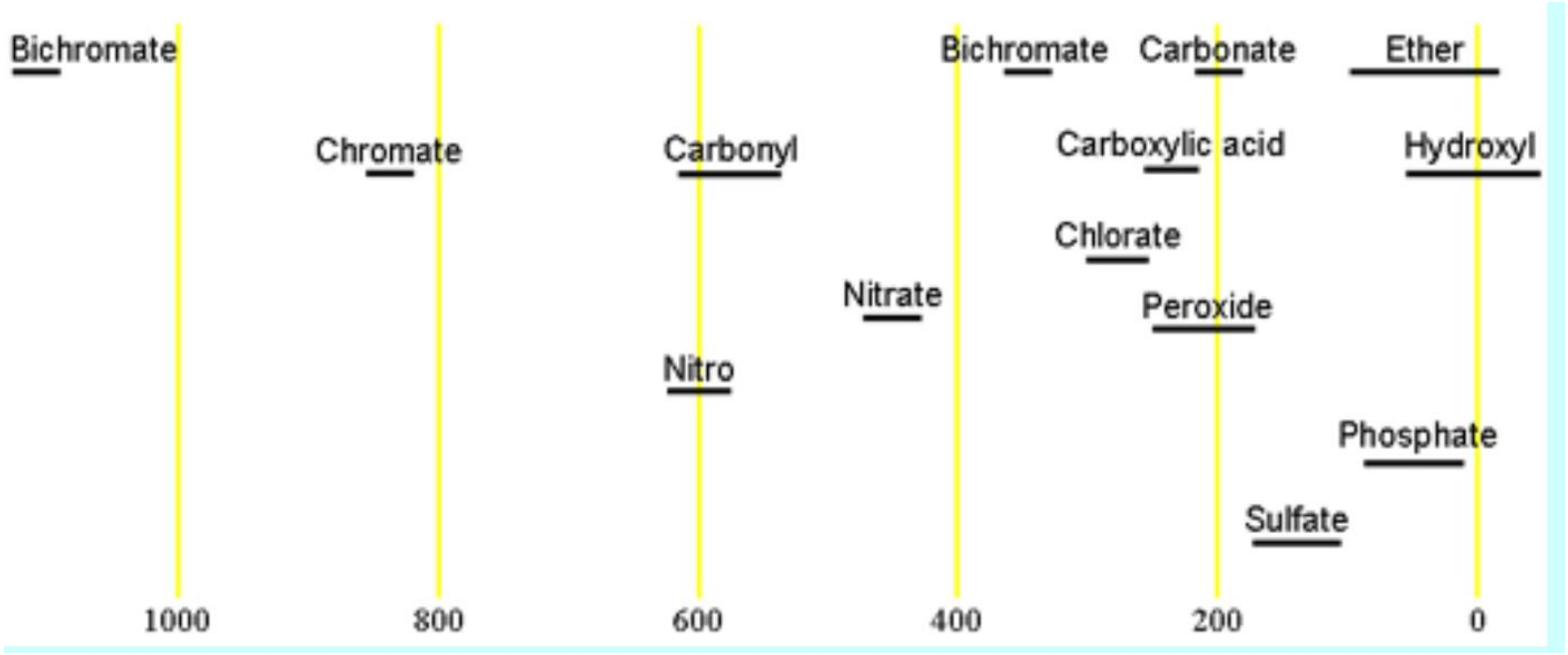

Multinuclear Magnetic Resonance (NMR)

Properties of ^{195}Pt

Property	Value
Spin	1/2
Natural abundance	33.832%
Chemical shift range	6700 ppm, from -6500 to 200
Frequency ratio (Ξ)	21.496784%
Reference compound	1.2 M Na_2PtCl_6 in D_2O
Linewidth of reference	5.3 Hz
T_1 of reference	0.4 s
Receptivity rel. to ^{1}H at natural abundance	3.51×10^{-3}
Receptivity rel. to ^{1}H when enriched	0.0104
Receptivity rel. to ^{13}C at natural abundance	20.7
Receptivity rel. to ^{13}C when enriched	61.2

Chemical Shift Ranges for Platinum NMR

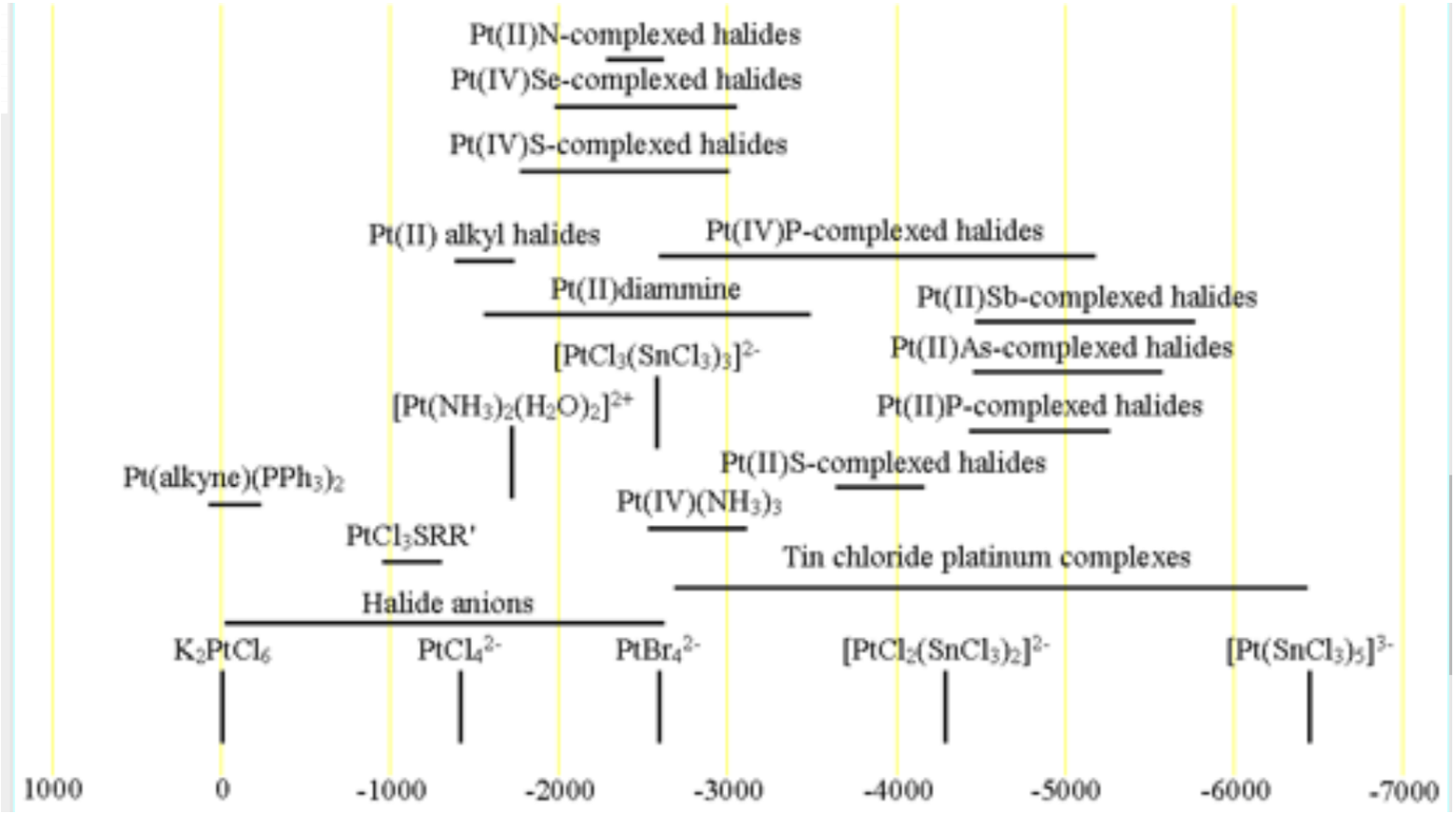

Multinuclear Magnetic Resonance (NMR)

Properties of ^{183}W

Property	Value
Spin	1/2
Natural abundance	14.31%
Chemical shift range	6720 ppm, from -4670 to 2050
Frequency ratio (Ξ)	4.166387%
Reference compound	1 M Na_2WO_4 in D_2O
Linewidth of reference	0.6 Hz
T_1 of reference	5 s
Receptivity rel. to ^{1}H at natural abundance	1.07×10^{-5}
Receptivity rel. to ^{1}H when enriched	7.48×10^{-5}
Receptivity rel. to ^{13}C at natural abundance	0.0631
Receptivity rel. to ^{13}C when enriched	0.441

Chemical Shift Ranges for Tungsten NMR

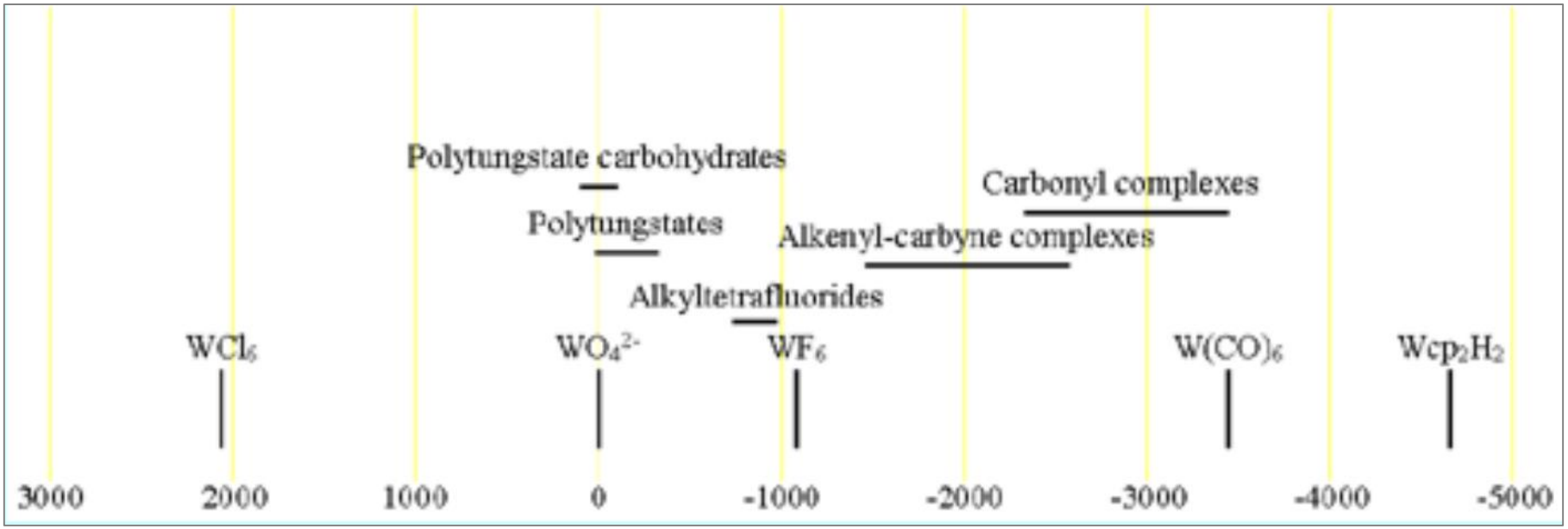

The ^{183}W NMR spectrum in H_2O/D_2O at room temperature.
JEOL ECX 400 instrument.
10 mm tube and Na_2WO_4 as 0 ppm reference.

^{183}W NMR Study in Solution

$[As^{III}_2W_{19}O_{67}(H_2O)]^{14-}$

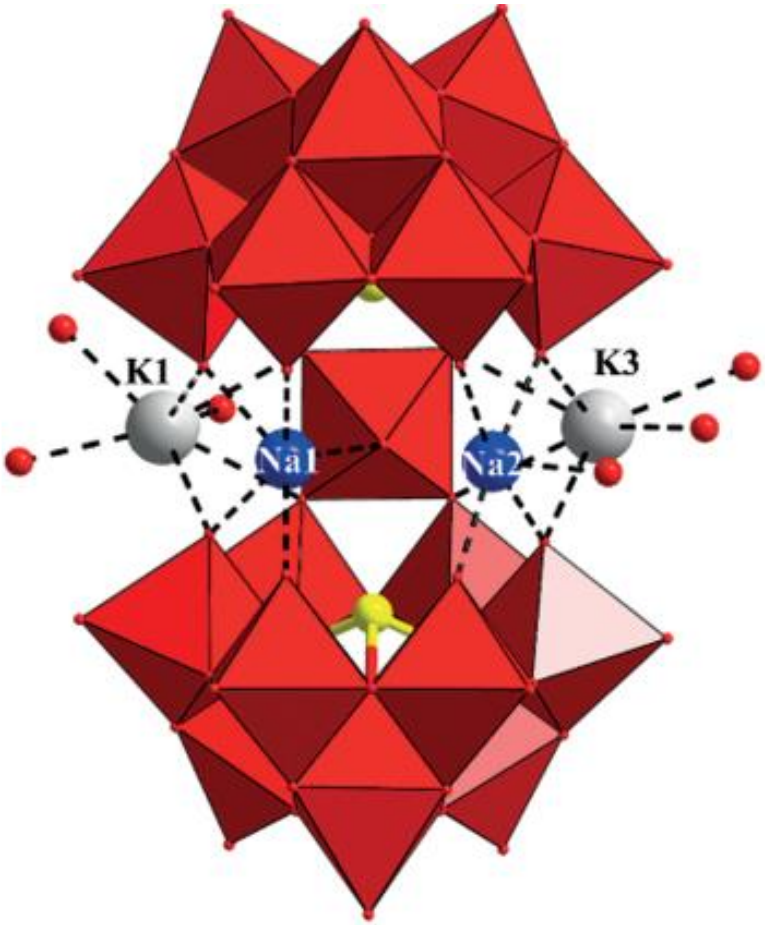

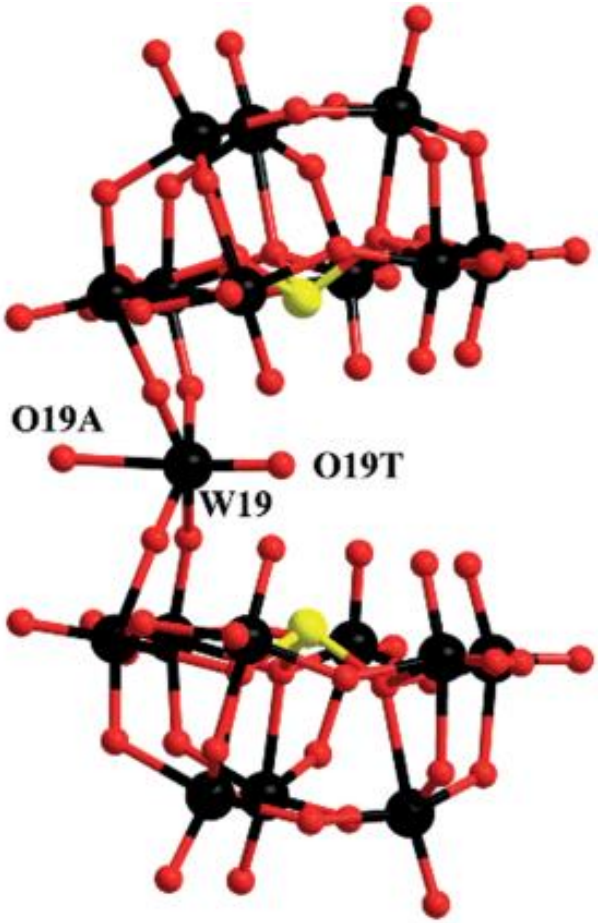

Wang, K.-Y., Bassil, B.S., Carey, A.M., Mougharbel, A.S. and Kortz, U. *Eur. J. Inorg. Chem*., 2017: 4210-4213

^{183}W NMR Study in Solution

$[As^{III}_2W_{19}O_{67}(H_2O)]^{14-}$

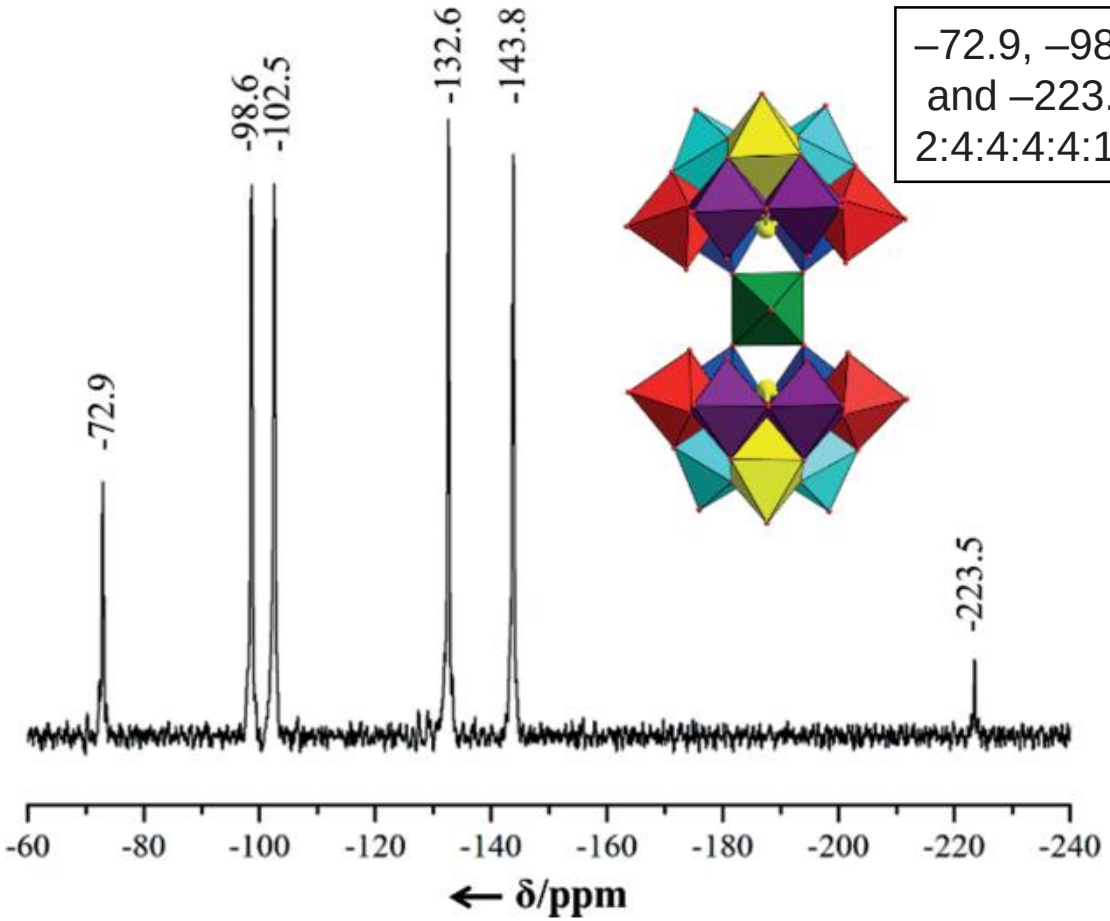

–72.9, –98.6, –102.5, –132.6, –143.8, and –223.5 ppm, with relative intensities of 2:4:4:4:4:1, respectively.

Inset: polyhedral representation with structurally inequivalent W centers shown in different colors.

^{183}W NMR Study in Solution

$[(LSb^{III})_4(A\text{-}\alpha\text{-}As^{V}W_9O_{34})_2]^{10-}$ (L = Ph)

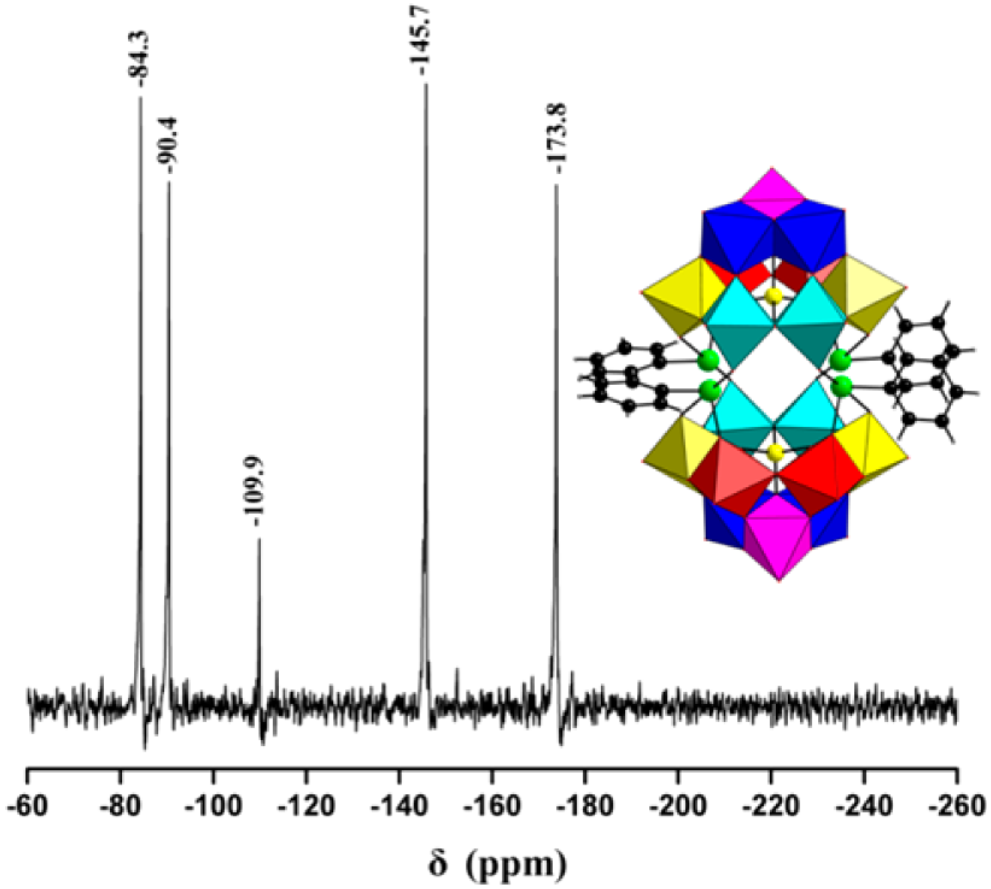

Five peaks with relative intensities 2:2:1:2:2

Equivalent WO_6 octahedra are shown in the same color.

Yang, P.; Lin, Z.; Bassil, B. S.; Alfaro-Espinoza, G.; Ullrich, M. S.; Li, M.-X.; Silvestru, C.; Kortz, U. *Inorg. Chem.* **2016**, *55*, 3718– 3720.

^{183}W NMR Study in Solution

$[Ce^{IV}_6(O_2)_9(GeW_{10}O_{37})_3]^{24-}$

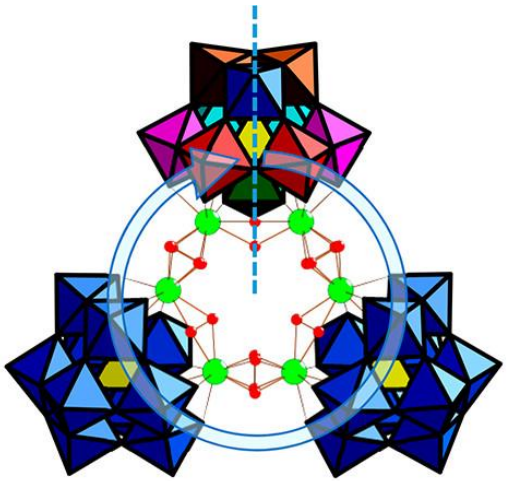

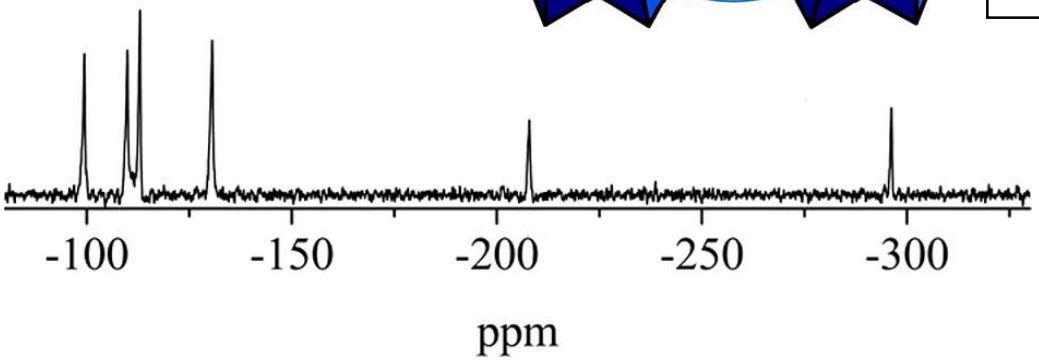

Six peaks at −99.4, −109.9, −113.0, −130.6, −207.9, and −296.2 ppm, with a 2:2:2:2:1:1 intensity ratio.

H. M. Qasim , W. W. Ayass , P. Donfack , A. S. Mougharbel , S. Bhattacharya , T. Nisar , T. Balster , A. Solé-Daura , I. Römer , J. Goura , A. Materny , V. Wagner , J. M. Poblet , B. S. Bassil and U. Kortz , *Inorg. Chem.*, 2019, **58** , 11300.

^{31}P NMR Study in Solution

$[P_2W_{18}O_{62}]^{6-}$

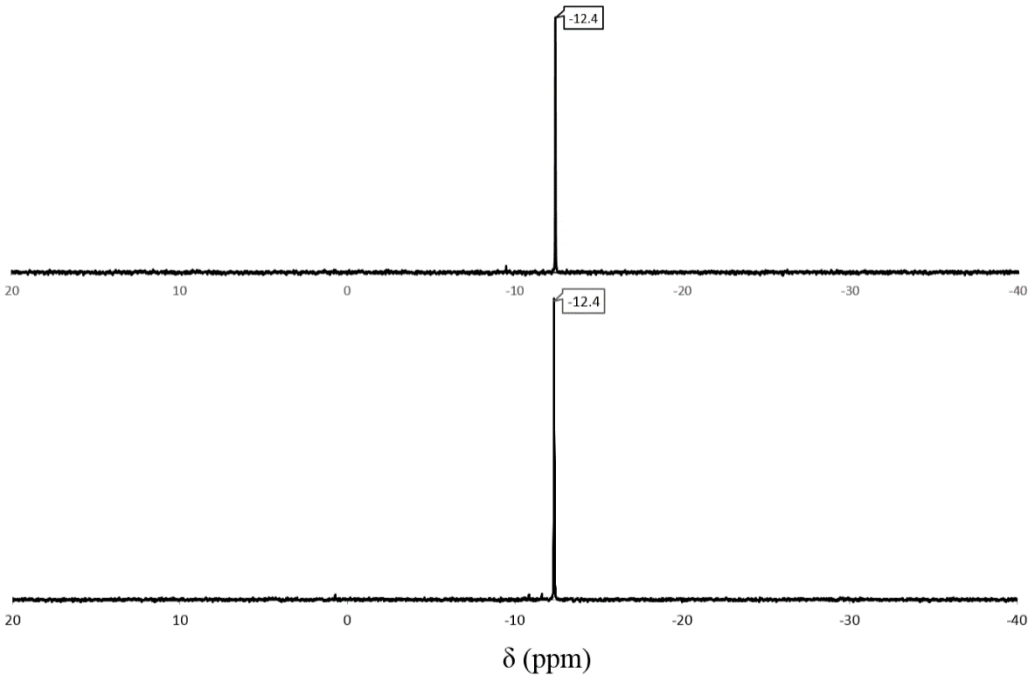

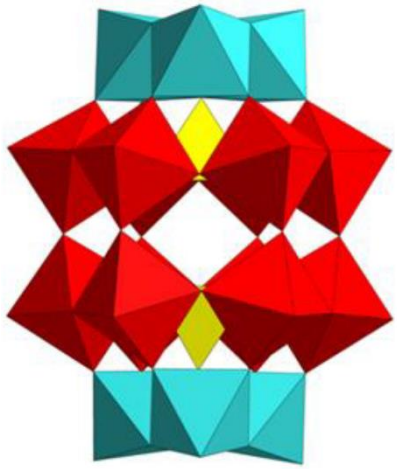

(lower) synthesized by microwave-assisted heating and (upper) by conventional heating.

Inorganics **2019**, *7*(2), 23; https://doi.org/10.3390/inorganics7020023

^{89}Y NMR Study in Solution

$[Y\{PM_2W_{10}O_{38}(H_2O)_2\}_2]^{11-}$ (M = Co^{II} and Zn^{II})

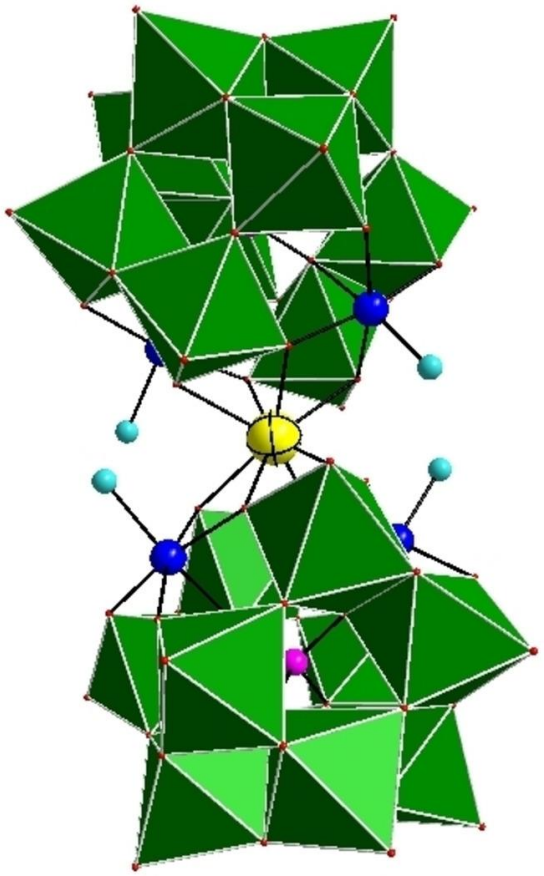

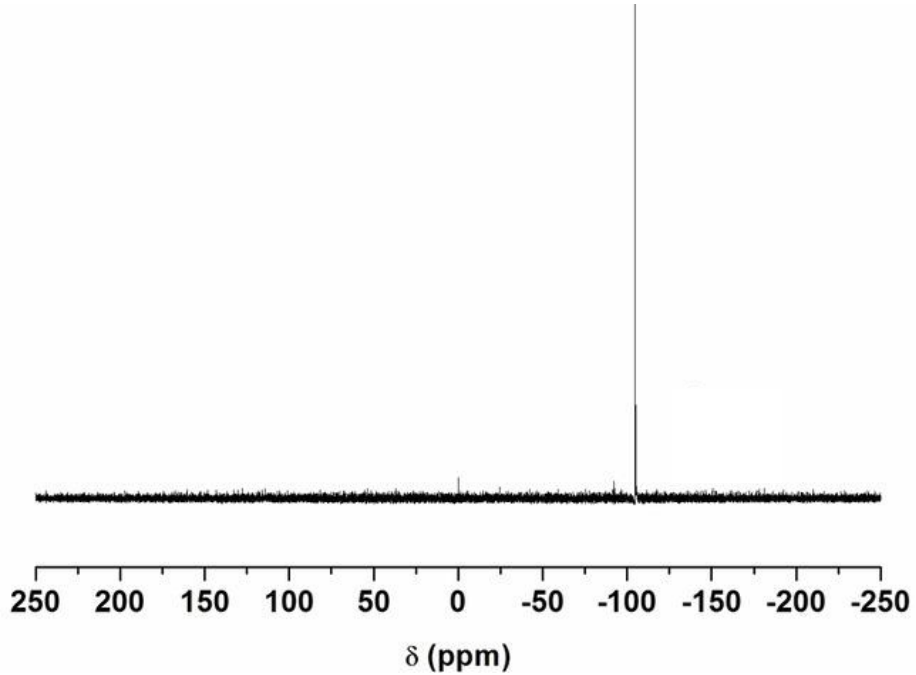

One signal at around −104.79 ppm and suggests that one yttrium ion is sandwiched between the two [α-$PW_{10}O_{36}$] units

V. Das, R. Gupta, N. Iseki, M. Sadakane, A. S. Mougharbel, U. Kortz, F. Hussain, *ChemistrySelect* **2019** , *4* , 2538.

^{51}V NMR NMR Study in Solution

The polyanion $[H_2Pt^{IV}V_9O_{28}]^{5-}$

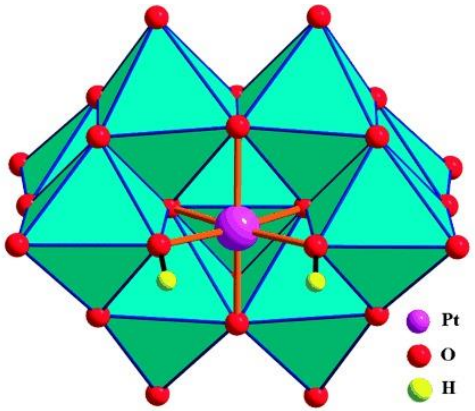

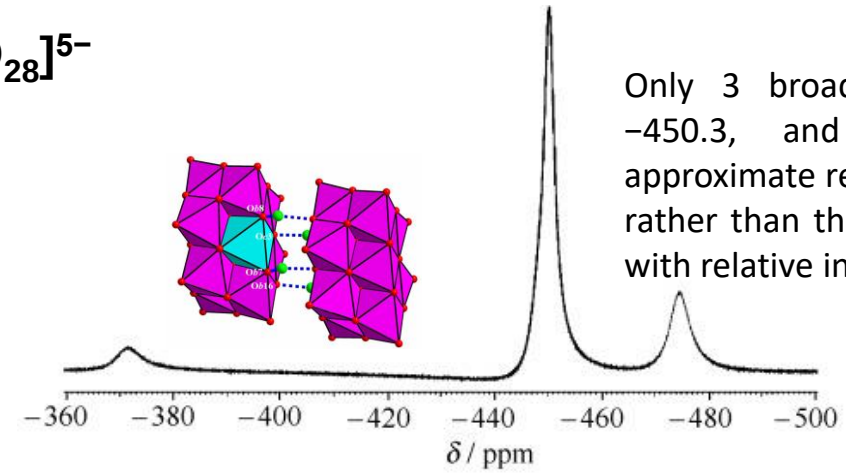

Only 3 broad peaks (δ =−371.4, −450.3, and −475.1 ppm) with approximate relative intensities 1:2:6 rather than the expected four peaks with relative intensities 1:2:2:4.

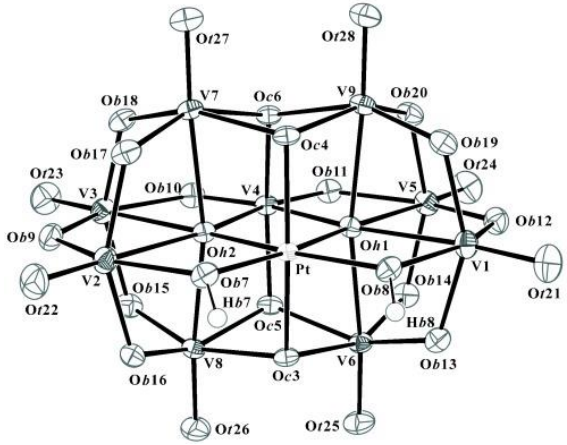

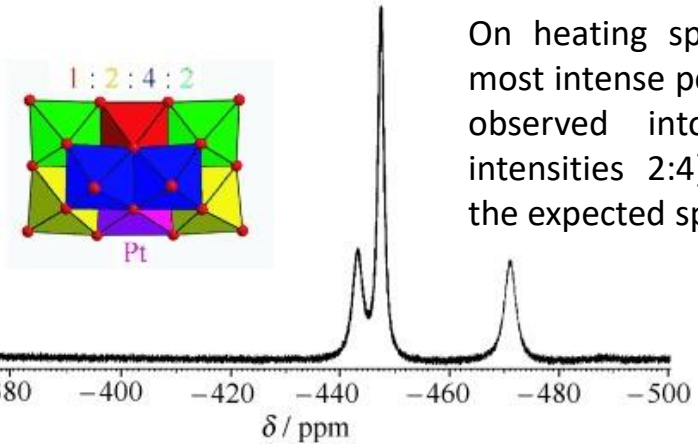

On heating splitting of the central, most intense peak (with intensity 6) is observed into two peaks (with intensities 2:4), resulting in exactly the expected spectrum.

^{51}V NMR spectrum of compound dissolved in H_2O/D_2O at 293 K (top) and 333 K (bottom).

U. Lee, H. C. Joo, K. M. Park, S. S. Mal, U. Kortz, B. Keita and L. Nadjo, *Angew. Chem. Int. Ed*, 2008, 47, 793– 796.

^{195}Pt NMR Study in Solution

The polyanion $[H_2Pt^{IV}V_9O_{28}]^{5-}$

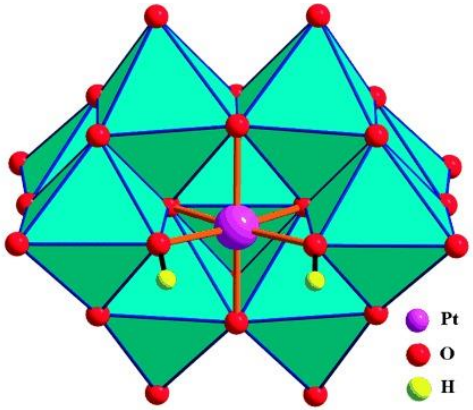

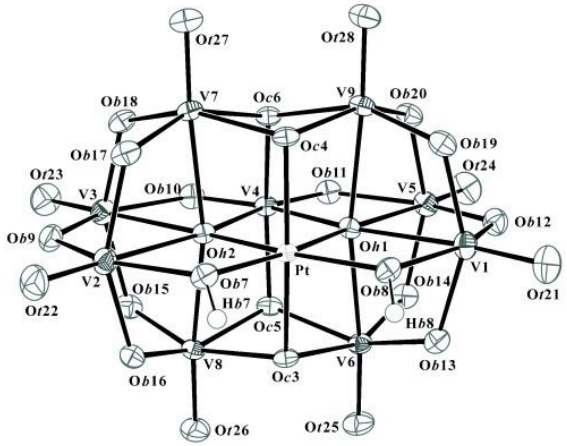

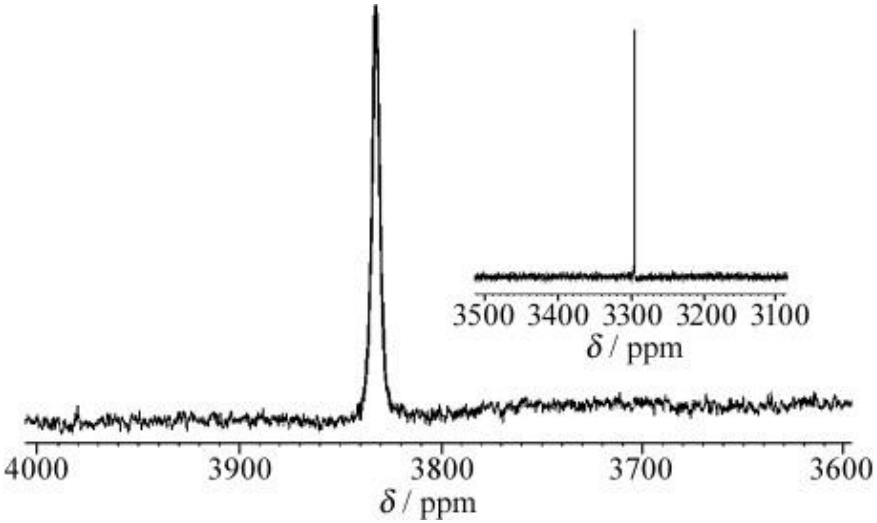

^{195}Pt NMR spectrum of compound and of the precursor $H_2[Pt(OH)_6]$ (inset) in H_2O/D_2O at 293 K.

U. Lee, H. C. Joo, K. M. Park, S. S. Mal, U. Kortz, B. Keita and L. Nadjo, *Angew. Chem. Int. Ed*, 2008, 47, 793– 796.

MAS ^{77}Se NMR Study

$[(Se_2W_{12}O_{46}(WO(H_2O))_3]^{24-}$

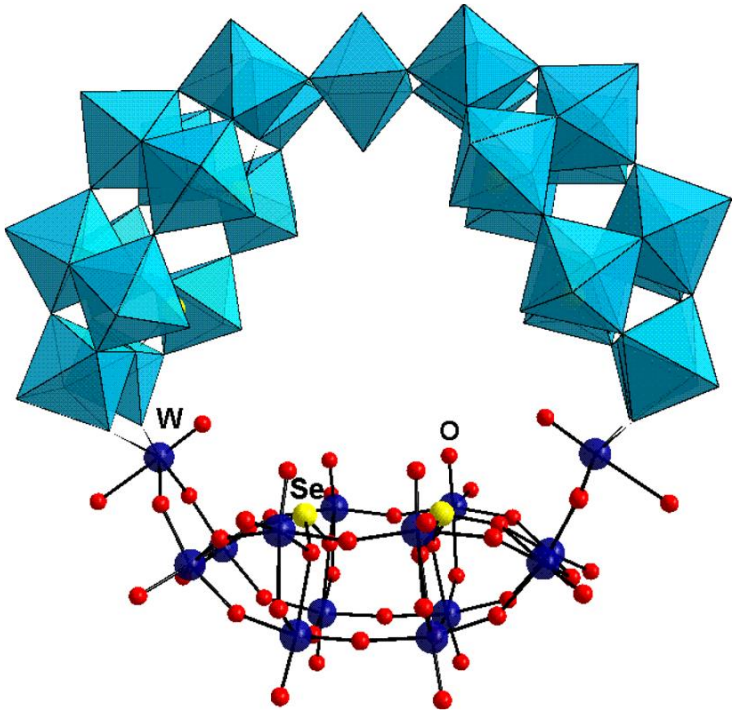

Color legend: WO_6, blue octahedra;
Se, yellow balls; W, blue balls; O, red balls.

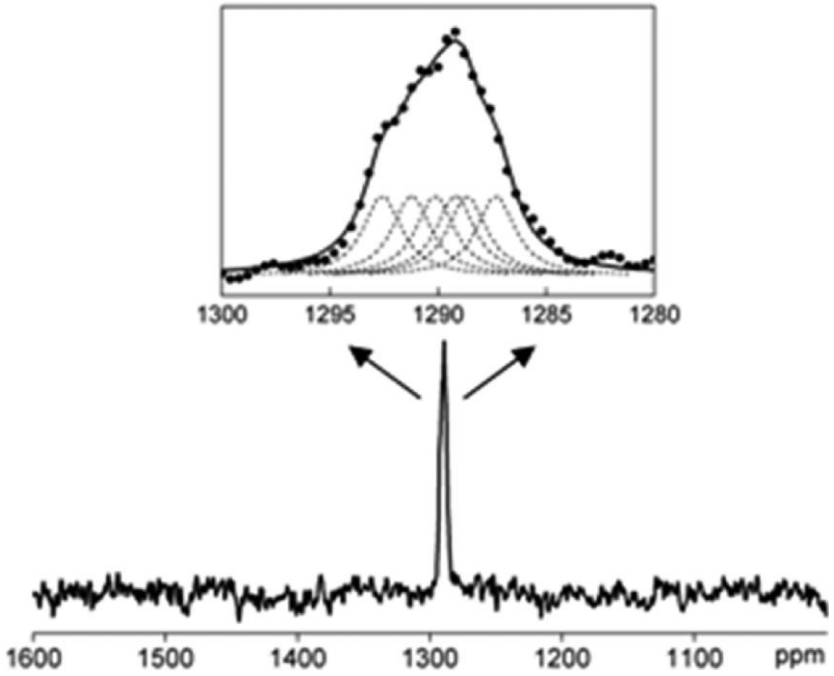

The experimental line shape and its representation as a superposition of six resonance lines, identical in widths and intensities, are shown in the inset by points and a solid line, respectively; the sextet components at 1287.3, 1288.7, 1289.2, 1290.1, 1291.2, and 1292.6 ppm are shown as dashed lines

Kalinina, I. V.; Peresypkina, E. V.; Izarova, N. V.; Nkala, F. M.; Kortz, U.; Kompankov, N. B.; Moroz, N. K.; Sokolov, M. N. *Inorg. Chem.* **2014**, *53*, 2076– 2082.

^{77}Se NMR Study in Solution

$[(Se_2W_{12}O_{46}(WO(H_2O))_3]^{24-}$

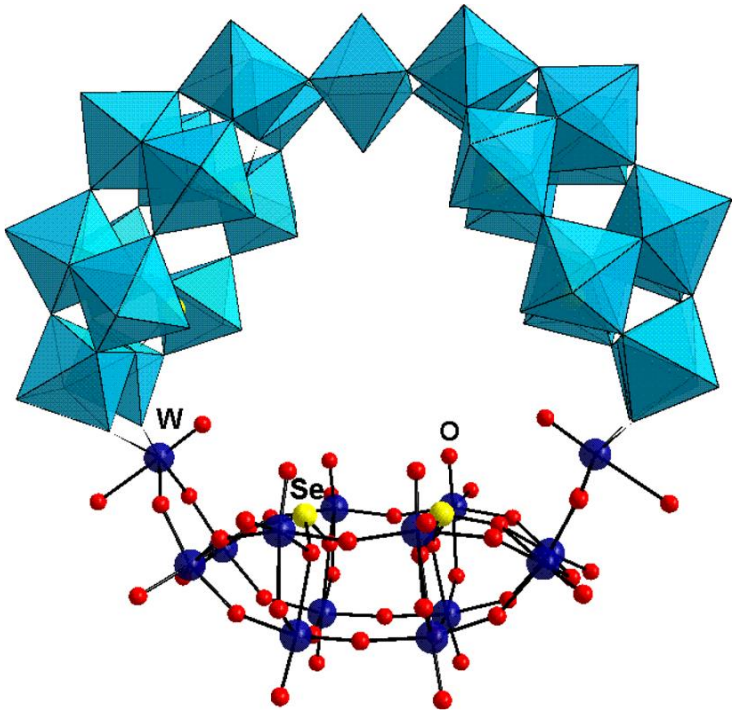

Color legend: WO_6, blue octahedra;
Se, yellow balls; W, blue balls; O, red balls.

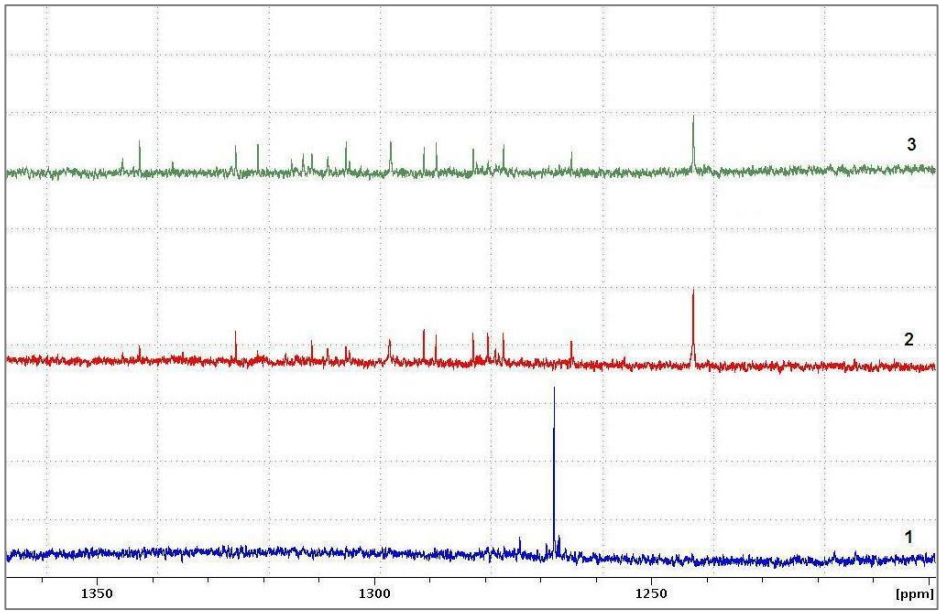

1.Spectrum recorded immediately after dissolution.
2. Spectrum recorded 4 h after dissolution.
3. Spectrum recorded 16 h after dissolution

Kalinina, I. V.; Peresypkina, E. V.; Izarova, N. V.; Nkala, F. M.; Kortz, U.; Kompankov, N. B.; Moroz, N. K.; Sokolov, M. N. *Inorg. Chem.* **2014**, *53*, 2076– 2082.

^{77}Se NMR Study in Solution

$MO_8Pd^{II}_{12}(SeO_3)_8]^{n-}$ (M= Zn, Lu)

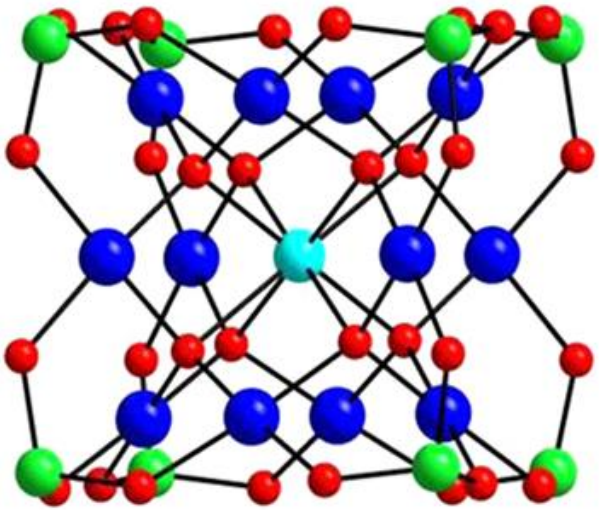

$[MO_8Pd^{II}_{12}(SeO_3)_8]^{n-}$ (Color code:
M, turquoise; Pd, blue; O, red; Se, green.

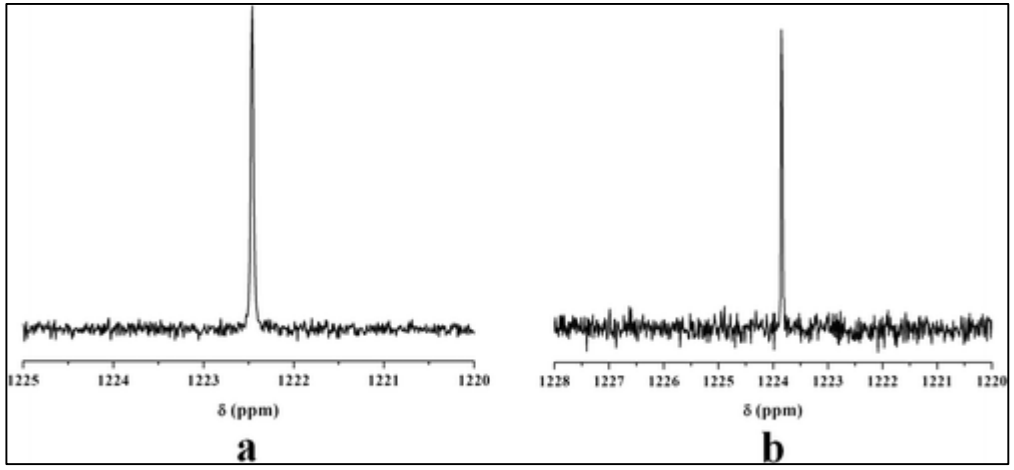

^{77}Se NMR spectra of **ZnSe** (a) and **LuSe** (b)

Barsukova-Stuckart, M.; Izarova, N. V.; Barrett, R. A.; Wang, Z.; van Tol, J.; Kroto, H. W.; Dalal, N. S.; Jiménez-Lozano, P.; Carbó, J. J.; Poblet, J. M.; von Gernler, M. S.; Drewello, T.; de Oliveira, P.; Keita, B.; Kortz, U. *Inorg. Chem.* **2012**, *51*, 13214– 13228.

^{27}Al NMR Study in Solution

Keggin-type aluminum polyoxocation

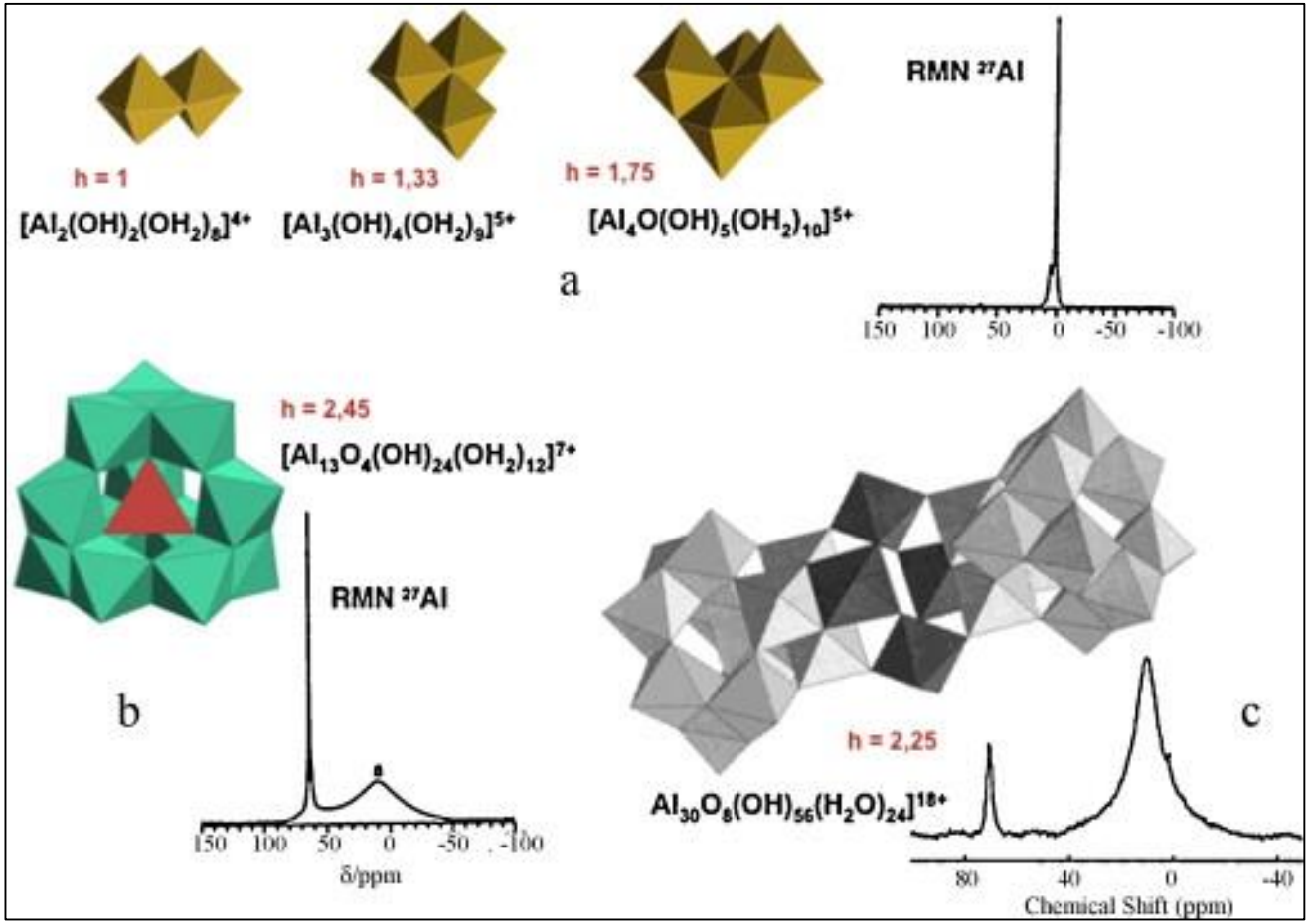

J.P. Jolivet, C. Chaneac, D. Chiche, S. Cassaignon, O. Durupthy, J. Hernandez, *Comptes Rendus Geosciences*, 2011, 343, 113-122

^{17}O NMR Study in Solution

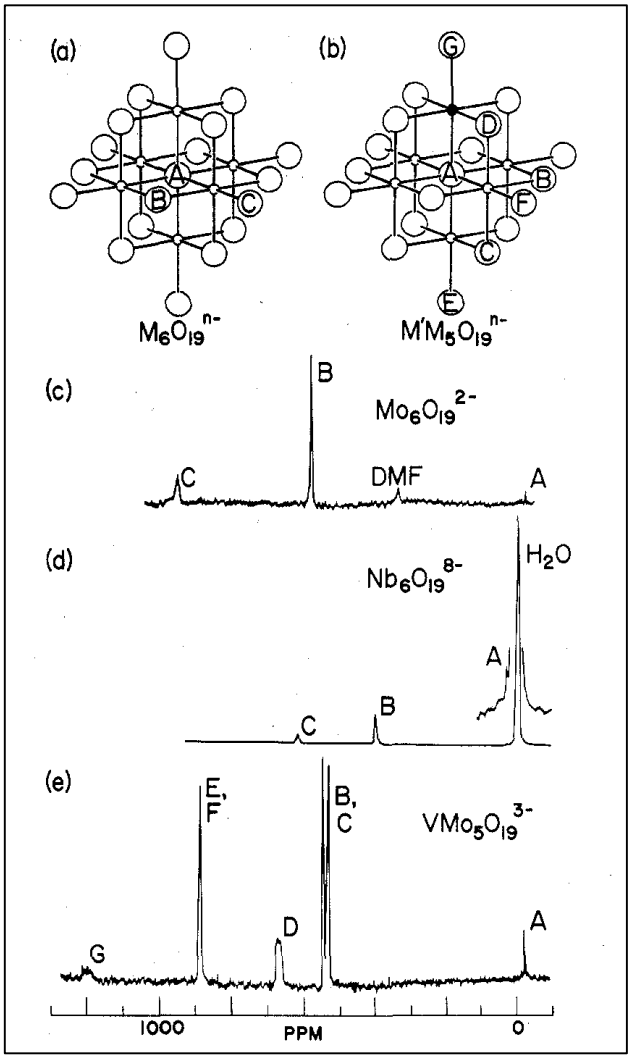

Inorganic Chemistry, Vol. 18, No. 1, 1979, 93

Lindqvist POM $[M_6O_{19}]^{n-}$ (M = Mo^{VI}, W^{VI}, Nb^{V}, and Ta^{V})

- Contain only three nonequivalent types of oxygens

- 6 terminal oxygens (O_C)
- 12 doubly bridging oxygens (O_B),
- Sixfold bridging oxygen (O_A).

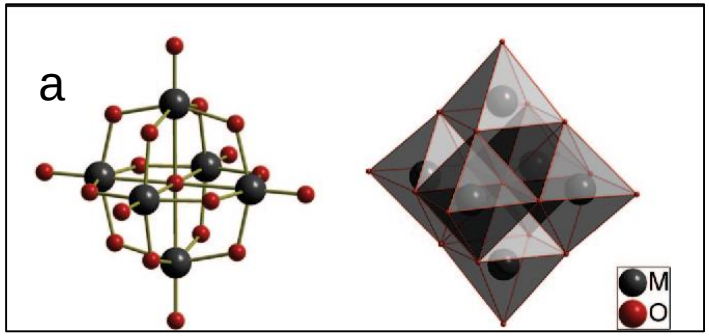

3 nonequivalent oxygens

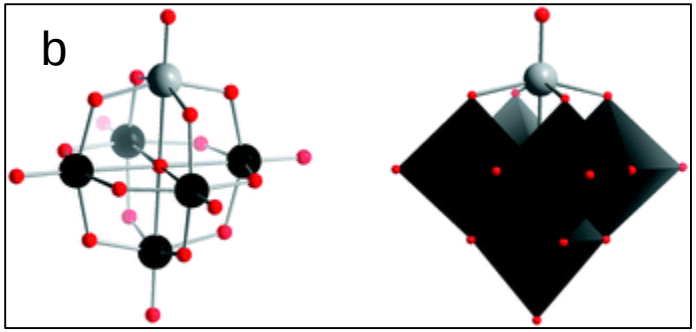

7 nonequivalent oxygens

Other Methods

POMs have a rich electrochemistry associated with both reduction of tungsten or molybdenum and redox-reaction of heterometals (i.e., incorporated cobalt, ruthenium, iridium, or nickel). These characteristic redox wave peaks can be used to identify the number of terminal oxygen atoms, metastable hydrolysis fragments, new isomers and reduced anions.

Extended X-ray absorption fine structure (EXAFS) and X-ray absorption near edge structure (XANES) are valuable techniques to probe both the local coordination environment and the oxidation state of POM's atoms either in solution or in solid-state materials. Each kind of atom in the POM cluster can be accessed individually and an average spectrum for each element is observed. Despite XAS (X-ray absorption spectroscopy) being a powerful technique, there are just a limited number of examples for their usage in POM structure analysis.

Dynamic light scattering (DLS) is aimed to determine whether particles are formed in solutions and, if present, to examine their size. DLS has found its broadest usage in monitoring POM stability during catalytic reactions (e.g. water splitting systems).